RIP CHANNEL MORPHODYNAMICS AT PENSACOLA BEACH, FLORIDA

A Thesis

by

DANIEL R. LABUDE

Submitted to the Office of Graduate Studies of
Texas A&M University
in partial fulfillment of the requirements for the degree of

MASTER OF SCIENCE

Approved by:

Chair of Committee,	Chris Houser
Committee Members,	Vatche Tchakerian
	Anthony Filippi
Head of Department,	Vatche Tchakerian

December 2012

Major Subject: Geography

ABSTRACT

80% of all lifeguard related rescues along the beaches of northwest Florida are believed to be related to rip currents. A rip current is the strong flow of water, seaward extending from the beach to the breaker line. It has previously been shown that there are rip current hot spots at Pensacola Beach, forced by a ridge and swale topography offshore, but the annual evolution/behavior of these hotspots (i.e. location, size, frequency, and orientation) have not been examined in detail. Remote imagery from Casino Beach was rectified to a planar view in order to examine the rip channel characteristics. These characteristics were analyzed to determine variations and patterns on a daily, monthly, and seasonal basis and in relation to reset storms, wind and wave characteristics, and the beach states of Casino Beach in order to characterize the rip development and variation throughout a year.

Beach states and rip configurations were impacted by many frontal storms and one tropical storm, which were classified as a reset storm when reconfigurations of the beach state and rips occurred. Given sufficient time between reset storms, the bar migrated onshore, transitioning from LBT, to RBB, and finally to TBR state. The lack of reset storms after March 2010 resulted in a large frequency of observed rip channels (64) between April and May. It is shown that these rip channels are clustered into 7 statistically significant groups based on their location alongshore at the 95 % confidence interval. It is argued that the rip channel clusters are a direct result of the wave forcing caused by the ridge and swale topography. This situation causes the bar to move

onshore that without interruption of a reset storm will attach at certain locations creating a transverse bar and rip morphology. The bar appears to attach to the beach at consistent locations throughout the year creating similar rip locations and subsequently the rip clusters. The risk posed to beach users by these rip currents is concentrated in certain locations which are persistent throughout the year.

DEDICATION

This thesis is dedicated to my entire family. Their patience, love, and support were instrumental in the work and dedication that was needed to complete the thesis. They have instilled in me the characteristics that have shaped me into the hard working patient, dedicated, and passionate person I am today.

ACKNOWLEDGEMENTS

I would like to thank my committee chair, Dr. Houser, and my committee members, Dr. Filippi, and Dr. Tchakerian, for their guidance and support throughout the course of this research.

Thanks also go to my friends and colleagues and the department faculty and staff for making my time at Texas A&M University a great experience. I also want to thank my brother Brian for being there with me along the way and providing encouragement and kick in right direction when needed.

Finally, thanks to my mother and father for their encouragement, support, and love, throughout this entire process.

TABLE OF CONTENTS

LIST OF FIGURES

FIGURE Page

LIST OF TABLES

CHAPTER I

INTRODUCTION

Between 2000 and 2009 there were 25 drownings at Pensacola Beach, Florida, all presumed to be a result of rip currents (Houser, Barrett and Labude, 2011). It has previously been shown that the rip currents at Pensacola Beach occur at hotspots forced by ridge and swale topography on the inner-shelf (Barrett and Houser, 2012: Houser, Barrett, and Labude, 2011). What has yet to be determined is how these rip currents are controlled, arranged, and structured within a given hotspot in response to variations in storm activity. Specifically, it is not clear how the location, size, orientation, and frequency vary within the hotspot over a year. Previous studies have examined rip currents (at a variety of locations) based on their type (Short, 1985), beach state (Brander, 1999; Short, 1985; Wright and Short, 1984), underlying topography (McMahan *et al*., 2005; Smit *et al*., 2007), velocities (Brander and Short, 2000; Brander and Short, 2001; McMahan *et al*., 2004 McMahan *et al*., 2005) and even the conditions that result in rip related fatalities (Houser, Barrett, Labude, 2011). This research will examine rip channel development in relation to the recovery of the nearshore following recent hurricane activity (2004/2005) and in response to storms during the 2009/2010 season. It is hypothesized that the present rip current hazard at Pensacola Beach is a response to the slow landward migration of the bars following extreme storms, leading to semi-permanent accretion rips. Welding of the inner sand bar to the beach creates a transverse bar and rip beach state (Wright and Short, 1984), which is the most common

beach state at Pensacola Beach (Barrett and Houser, 2012) . The behavior of the bar system at Pensacola Beach and the development of rips is most likely related to local wind and wave forcing, but due to variations in storm activity the timing, frequency, and other rip characteristics vary annually.

There have been only a few studies that have looked at the relationship between beach recovery and the development of semi-permanent rip currents (e.g. Brander, 1999; Wright and Short, 1984). Beach recovery as defined by Brander (1999) and Wright and Short (1984) is the continuous migration of the sand bar onshore until the bar fully attaches to the beach. As sand bars migrate onshore the beach goes through numerous states: dissipative, intermediate (which includes longshore bar and trough, rhythmic bar and beach, transverse bar and rip, and low-tide terrace), and reflective (Figure 1). The intermediate state results in the strongest of rip current activity because the rip channels are better defined and more persistent than the other beach states (Brander, 1999; Wright and Short, 1984). Of the stronger rip current activity the best formed and strongest of rips occur in the transverse bar and rip state as a result of the rip channels being the most defined and not as wide as other beach states (intermediate), while the largest but weakest rips result at longshore bar and trough beach states (Brander, 1999; Wright and Short, 1984). As the beach state moves from the longshore bar and trough, to low-tide terrace the rip channels decrease in width, but increase in strength (Brander, 1999;

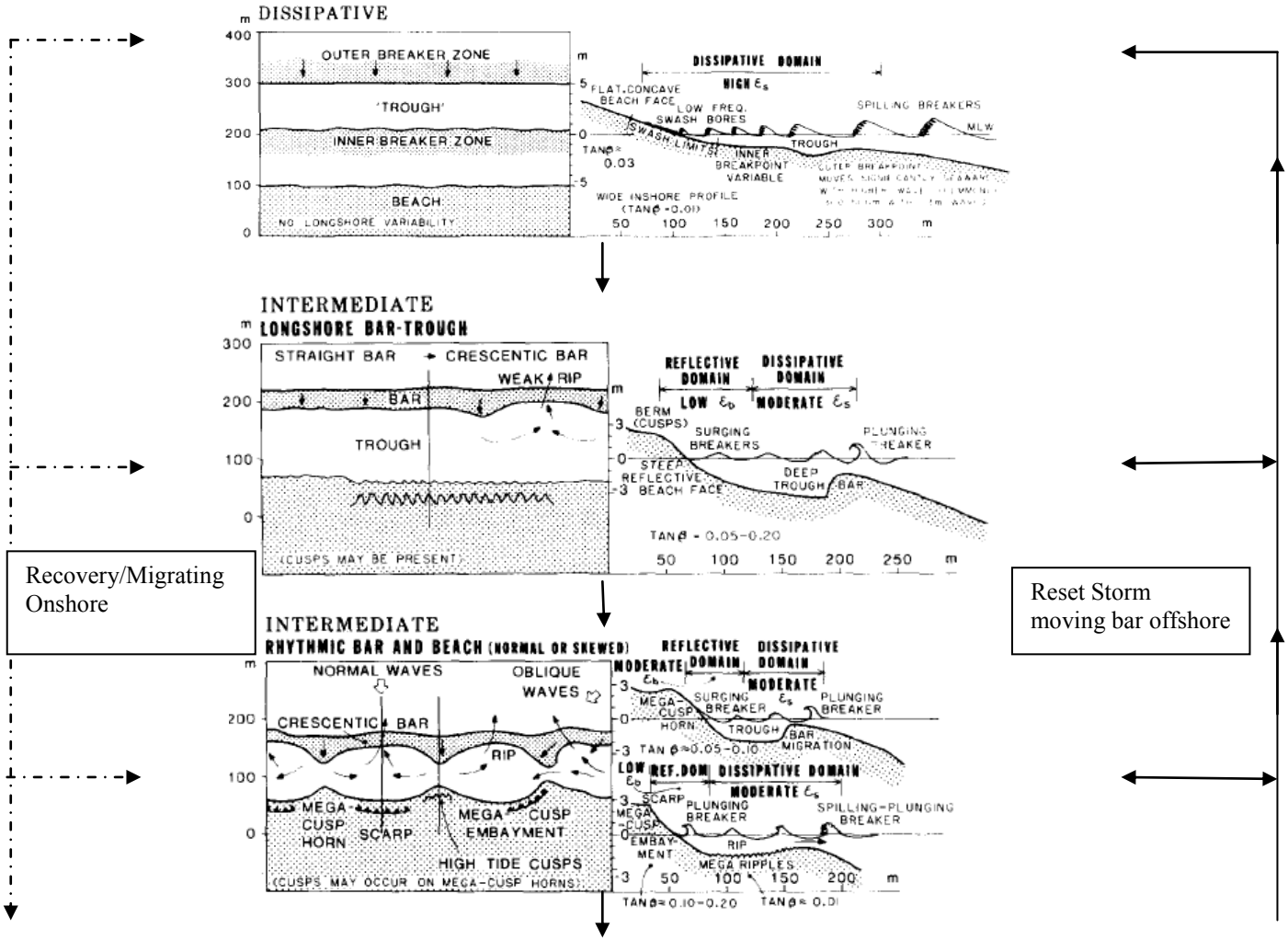

Figure 1: Beach state morphologies. Modified from Wright and Short (1984). Dashed line represents the bar migration during recovery, while the solid lies on the right represent reset storms moving the bar offshore.

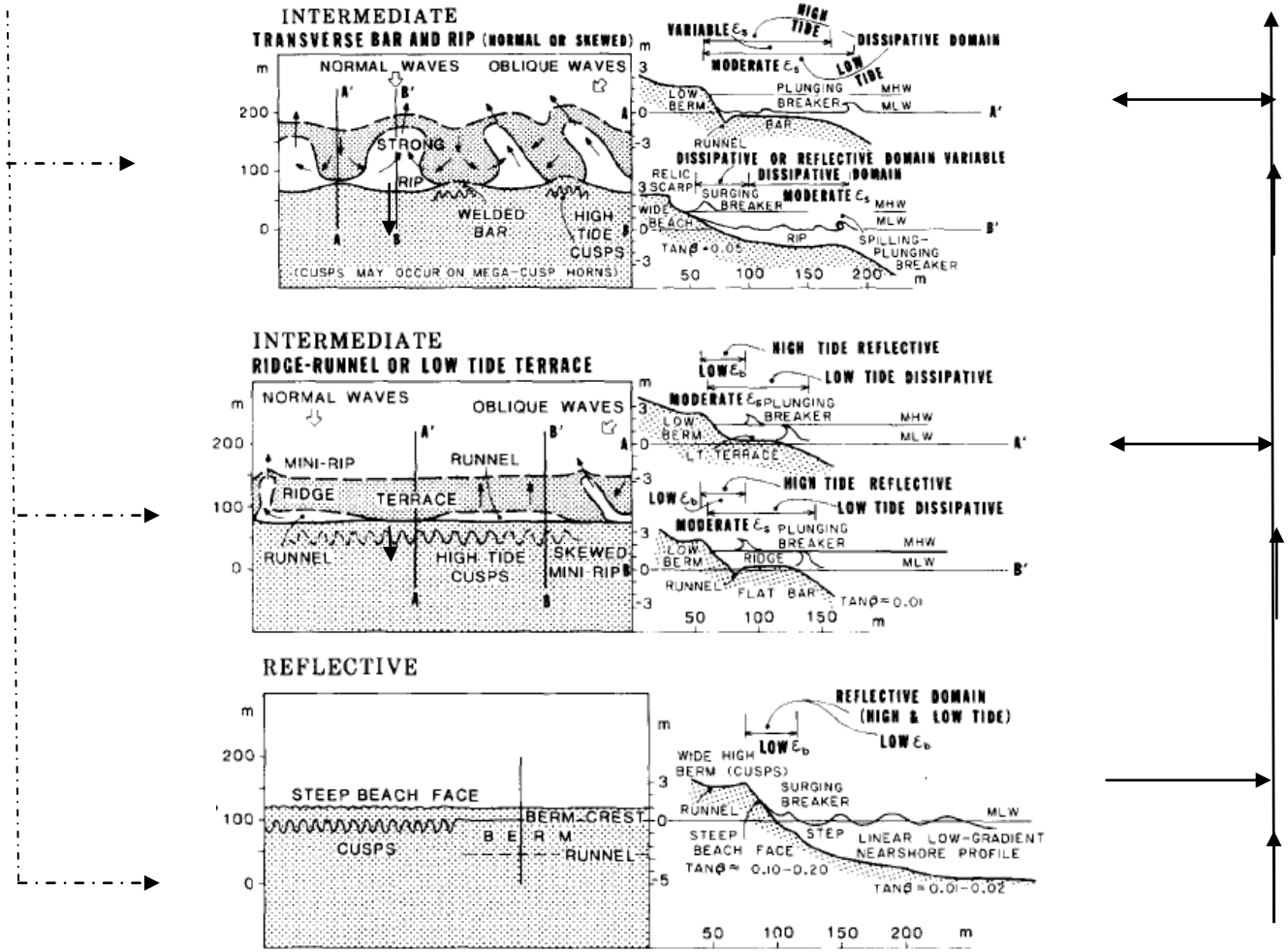

Figure 1 Continued

Wright and Short, 1984). A reflective beach state develops as the beach fully recovers and the bar welds to the beach (Brander, 1999; Wright and Short, 1984). The nearshore will remain in the state until a reset storm moves the sand bar back offshore and the cycle begins again (Wright and Short, 1984). This cycle can however be interrupted or reset at any point in time based on the timing of storms.

Beach state and nearshore morphology can be examined through the use of remote imagery and analysis. Specifically, remote sensing can be used to examine how and where rip channels develop, including their location, size, and frequency. This type of information will also provide safety officials at Pensacola Beach, Florida with information to help them properly allocate funds and personnel in the hopes of saving lives, by knowing where and under what conditions rip currents are most likely to form at Casino Beach. The specific objectives of this study are to:

- Quantify and characterize the behavior and development of accretion rips at Casino Beach over a year (September 2009 – September 2010), and
- Determine the variation in rip hazard over a year (September 2009 – September 2010). The variations will be examined in relation to changes in the frequency, area, angle, and condition under which the rips develop will be examined.

CHAPTER II

LITERATURE REVIEW

2.a Natural Hazard

A natural hazard is a naturally occurring phenomenon that results in a substantial impact on the environment as well as human life (Short and Hogan, 1994). Natural hazards come in all forms, from tornadoes, hurricanes, earthquakes, floods, to lightning. The natural hazards listed above, with the exception of lightning, are high magnitude, low frequency hazards. For example, there were only 1282 recorded tornadoes in 2010 and 0 land falling hurricanes in the U.S. (NOAA, 2011). They impact humans on a large scale, but do not occur frequently. These large natural hazards generally receive the most attention by the national media and the government. Natural hazards that occur on small scales such as rip currents receive far less attention, even though rip currents generally result in more deaths than many of the above mentioned natural hazards. According to NOAA, rip currents are rated as the natural hazard that results in the third most deaths per year in the United States, only floods and heat cause more deaths (Figure 2). Rip currents are believed to be responsible for 100 deaths per year, along the

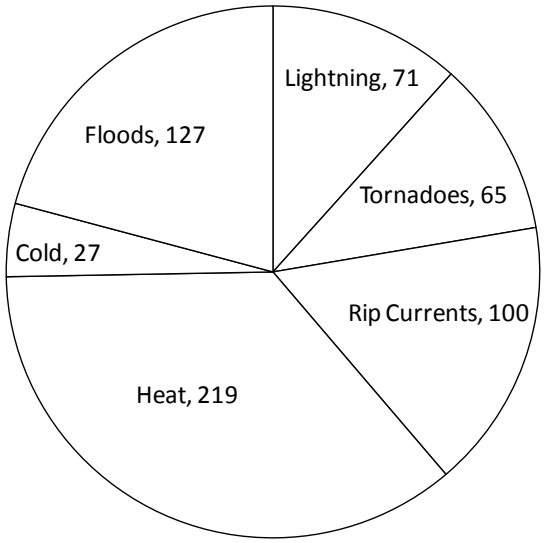

Figure 2: Pie chart showing the number of deaths annualy related to the top 6 hazards in the United States (NOAA).

beaches of the United States, second only to heat (219) and floods (127). In this respect, they are responsible for more deaths per year than lightning (71), tornadoes (65), and the cold (27) (NOAA, 2002). Other research has shown that the number of deaths per year related to rip currents in the United States has been near 150 per year (Lushine, 1991). Based on these statistics rip currents are a significant coastal hazard.

Based on Short and Hogan (1994), a "coastal" hazard is any phenomenon that puts a beach user into a dangerous condition that may result in them drowning. Rip currents require a perfect storm of beach conditions along with the right beach goer to cause harm. Social controls such as swimming ability, consumption of alcoholic beverages, age, health, gender and common sense all are key components that impact the

amount of risk posed to a given beach goer (Gensini and Ashley, 2009; Lushine, 1991). While difficult to quantify, it is believed that rip currents are associated with 80% of all rescues undertaken by lifeguards (Lascody, 1998; Lushine, 1991), similar to the national average across the United States (NOAA). The Florida Panhandle and Pensacola Beach were deemed one of the most dangerous beaches by the National Lifesaving Association of America in 2002 following 23 deaths related to rips in 2002. (The Tuscaloosa News, 2002). There were approximately 12,000 preventative acts taken by lifeguards along with 633 rescues at Pensacola Beach from 2004 to 2009 (Houser, Barrett, and Labude, 2011). There were also 25 drownings between 2000 and 2009. The high number of preventative acts, rescues and drownings combine to make Pensacola a dangerous beach. Compared to California the rip related rescues may seem low. This is because the number of beach users, wave heights, and the strength of rips in California are much greater than in Florida.

The number of people at risk to this hazard in the United States and at Pensacola Beach is increasing due to recent development along the coastlines of the United States, which brings in more tourists and residents each year in the United States (Short and Hogan, 1994). At Pensacola Beach there are approximately 1.8 million visitors every year (Houser, Barrett, and Labude, 2011), of which 2,500 per year will be in some type of risk that will require a preventative act/rescue from the lifeguards. The rip current hazard is primarily a threat during summer months due to the increase of tourist that travel to the beach along with the beach state and weather conditions associated with the spring and summer months (Gensini and Ashley, 2009; Short, 1985; Short and Hogan,

1994; Wright and Short, 1984). Specifically, summer weekends with onshore winds result in the largest risk of rip current fatality (Gensini and Ashley, 2009). Approximately 70% of rip current related fatalities occur during days with onshore winds, which result due to surface high pressure systems (Gensisni and Ashley, 2009). The rip current hazard is larger in the summer due to the wind speed and direction onshore along with the large amounts of people that will enter the water compared to the winter months (Gensini and Ashley, 2009). Also, the calmer the summer months are the more accretion occurs with the bar migration onshore with increased numbers of rips until the bar attaches to the shoreline (Gensini and Ashley, 2009; Short, 1985)

2.b Wave Set-up

As waves approach the shoreline they transform by shoaling and eventually break (Bagnold; 1946; Guza and Bowen, 1976; Shibayama, 2009). Wave breaking occurs as the wave interacts with the seafloor resulting in a decrease in the wave celerity, a decrease in wavelength, and an increase in wave height (Bagnold; 1946; Guza and Bowen, 1976: Shibayama, 2009). The wave will break at a threshold, which is characterized by a ratio of wave height to water depth. If the ratio gets to 0.8 the wave will begin to break (Bagnold; 1946; Shibayama, 2009). The momentum and energy associated with the breaking waves result in wave set-up, the slope or positive change in the mean water level within the surfzone (Bowen, Inman, and Simmons, 1968; Guza and Thornton, 1981; Longuet-Higgins, 1983; Svendsen, 1984). If one assumes that the mean

water level in the absence of waves as static, the momentum and energy cause the static mean water level to fluctuate in the presence of waves (Dean and Walton, 2009). Wave set-up is larger over a sand bar than inside a rip channel because the wave heights are larger over the bar than within the rip channel (Sonu, 1972; Wright and Short, 1984). The sand bar has a much shallower water depth to the sea floor then the area in the rip channel, which is much deeper causing the waves to be larger over the sand bar (Shibayama, 2009; Sonu, 1972). The difference in wave set-up forces a current which flows from the area of higher wave set-up (across the bar) to the area of lower wave set-up (rip channel) (Sonu, 1972). Sonu (1972) determined whether or not wave set-up and set-down was present over a sand bar. The experiment used water-filled polyethylene balls placed in the nearshore to monitor circulation patterns. The polyethylene balls flowed over the sand bar and toward the rip channel. When the balls converged at the rip channel, they flowed seaward through the rip channel. The experiment was conducted on the inner bar of a double sand bar system located at Seagrove, Florida. The inner bar exhibited features consistent of a rhythmic bar and beach state. The final results demonstrated that the polyethylene balls flowed from the area of higher surface gradient (over the bar) to the area lower surface gradient (the rip channel), showing that there was a current that could only be explained by wave set-up.

Standing infragravity waves add to the wave set-up resulting in periodic pulses of increased current velocity (Brander and Short, 2001). Infragravity waves occur at frequencies of 0.003 to 0.03 Hz, which is at much larger frequencies than incident waves (Holman, 1981). These infragravity waves can be linked to patterns found in higher

frequency wave groups (Holman, 1981). The excess momentum in the wave groups causes energy that creates infragravity waves from incident waves (Longuet-Higgins and Stewart, 1962). The influence of infragravity waves on the wave set-up occur at a different time scale than that of the normally breaking waves and the subsequent current, causing pulses in the wave set-up and current. (Brander and Short, 2001; MacMahan *et al*., 2004; Sonu, 1972). The infragravity waves can cause a change in the mean rip velocity by 0.25 m/s and a change in the instantaneous maximum velocity by 0.5 m/s (Brander and Short, 2001). The influence of wave set-up and infragravity waves on rip velocities is dependent on the nearshore morphology present on a given beach.

2.c Nearshore Morphology

2.c.1 Beach States and Rip Current Types

Rip currents are a strong flow of water, extending seaward from the beach to the breaker line. Rip velocities have been estimated at 0.1-1 m/s, although mega-rips can exceed 2 m/s (MacMahan, Thornton, and Reniers, 2006). Rips can be categorized into three types, erosion, accretion, and mega rips (Short, 1985). Erosion and accretion rips are found commonly with differing beach states (Short, 1985). As noted, there are three types of beach states, with the intermediate beach state usually resulting in the greater probability that accretion rips will develop (Wright and Short, 1984). The greater probability of rip development results due to differences in wave set-up across the

nearshore bar. The wave set-up over the bar is larger than that of the wave set-up between breaks in the bar (Sonu, 1972; Wright and Short, 1984), which leads to the development of a quasi-steady current through the gap in the nearshore bar (Sonu, 1972; Wright and Short, 1984). As shown in Figure 3, the intermediate beach state is categorized into four sub-states based on Wright and Short (1984): Longshore Bar and Trough (LBT), Rhythmic Bar and Beach (RBB), Transverse Bar and Rip (RBB), and Low Tide Terrace (LTT). The LBT beach state (Figure 3) is characterized by a longshore bar and trough with an occasional weak rip (Brander, 1999; Wright and Short 1984). The RBB beach state (Figure 3) has a crescentic bar along with a trough and more frequent rips (Brander, 1999; Wright and Short 1984). The TBR beach state (Figure 3) is characterized by a nearshore bar that has partially welded to the shoreline resulting in stronger more frequent rips (Brander, 1999; Wright and Short 1984). The higher frequency and stronger rips occur as a result of the rip channel width decreasing as the bar begins to weld to the beach increasing the rip velocity (Short, 1985). The last intermediate beach state is the LTT (Figure 3), which results when the bar is almost completely welded to the shoreline (Brander, 1999; Wright and Short 1984).

Strong rip currents can be found with a transverse bar and rip state (intermediate beach state) and are usually formed one to two weeks after maximum wave events (van Enckevort and Ruessink, 2003). In some cases, one to two weeks is enough time for the beach to recover and change from a LBT beach state to that of a TBR (van Enckevort and Ruessink, 2003). The reflective beach state can occasionally have rip currents develop, but this is not a constant phenomenon due to a lack of channel morphology that

is influential in the generation of rips (Short, 1985). Without the channel morphology, the differences in wave set-up needed to create the flow of water and the resulting rip currents are not usually present. However, the natural occurring bathymetry can cause a difference in wave heights alongshore, which can cause the needed difference in wave set-up to generate a rip. Dissipative beach states are not dominated by rips, but do have occasional erosional rips form (Short, 1985). The above beach states are in continuous motion from one to the other depending on the environmental conditions.

Changes from one beach state to another usually occur after storm events (Short, 1985; Wright and Short, 1984). When tropical cyclones or frontal storms strike, the bars located in the nearshore can be moved offshore (Sallenger Jr, Holman, and Birkemeier, 1985; Short, 1985). When this happens, the beach state is changed from an intermediate or reflective state to that of a dissipative state. As the bars migrate back onshore the beach state changes from dissipative to intermediate. Finally, when the bars attach to the beachface it becomes a reflective beach state (Short, 1985). This same pattern can be seen in Brander and Short (2001). In their experiment, the beach being examined (Palm Beach, New South Wales, Australia) started at a longshore bar and rip state following a storm. Over the course of their experiment the bar slowly migrated onshore changing the beach state. The beach state morphology went from the longshore bar and trough to a transverse bar and rip, and then finally to a low-tide terrace. The changes in beach morphology coincided with a dramatic decrease in energy following the storm observed at the beginning the experiment. Their study reinforced the model shown by Short (1985), which showed that after a reset of the bar/rip morphology the bar can move back

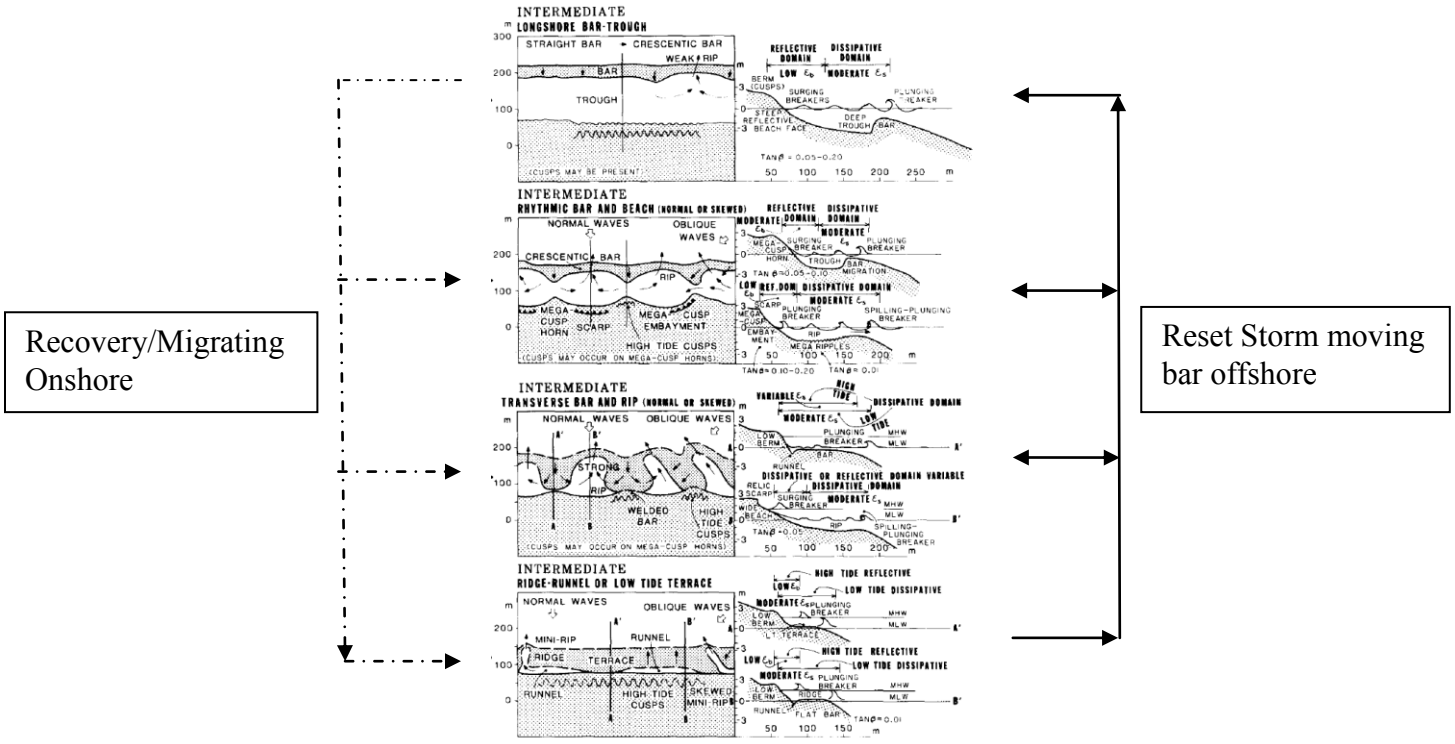

Figure 3: Intermediate beach state morphologies. Modified from Wright and Short (1984). Dashed line represents beach recovery and bar migration onshore. The Solid lines represent bar migration offshore due to reset storms.

onshore leading to different beach states and bar/rip morphology. Other studies, such as Kroon *et al.* (2007) have shown that following storms, beaches continue to recover during the lower energy environments and eventually the beach will develop an embayment and horn (i.e. transverse bar and rip) morphology.

Van Enckevort and Ruessink (2003) discovered that as bars migrate either onshore or offshore, the rip channels found in that area were greatly affected. As storms moved the sand bars offshore, the rip channels vanished and reappeared in new locations

as the bars migrated back onto shore. Following the storms the sand bars continued to migrate onshore. Strong rips formed when the beach changed from a crescentic bar state to a transverse bar and rip state, which occurred when the horns of the crescentic bar welded onto the shore. When the inner bar fully attached to the shore many of the rip currents vanished completely as the beach became reflective. The above studies show that accretion rips are more frequent and pose much more of a risk following storms.

Accretion rip currents form as a result of an alongshore variation in bathymetry, which cause a difference in wave set-up between the bar and rip channel similar to that of the formation of erosional rips (MacMahan *et al*., 2005). An alongshore current then forms, which moves from the area of larger wave set-up (the bar) to the area of lower wave set-up, the rip channel (MacMahan *et al*., 2005). The current then flows through the rip channel (MacMahan *et al*., 2005). The alongshore current is forced by the pressure gradient and radiation stress gradient acting together to move water from the area of high waves to the area of lower waves (MacMahan, Thornton, and Reniers, 2006). Accretion rips are found along intermediate beaches, which are areas that are actively accreting and with $\Omega < 2.5$ (Short, 1985). Accretion rips are usually persistent and last anywhere from a few days to a few weeks depending on the wave conditions and range anywhere from 10 meters in width to a few hundred meters (Short, 1985). Their velocities can vary, but are usually between 0-0.5 m/s (MacMahan, Thornton, Reniers, 2006; Short 1985).

2.c.1.a Erosion Rips

Erosion rips develop in response to high energy waves usually occurring during storm events (Short, 1985). The high energy waves and bathymetry cause a difference in wave set-up which forms a current and flows seaward eventually leading to a rip channel and current (Short, 1985). Similar to accretion rips, the rip channels result in the continued difference in wave set-up and causes an alongshore current to prolong, which flows towards the rip channel and then seaward as a rip current. Erosion rips are not permanent or semi-permanent like accretion rips. Unlike accretion rips, erosion rips are found in areas that the beach is generally eroding with $\Omega > 2.5$ and they can occur under any beach state (Short, 1985). The erosion rip is short lived, anywhere between a few hours to a few days (Short, 1985). This is due to being caused solely by the wave climate and bathymetry. When the wave climate is no longer conducive to generating a difference in wave set-up the erosion rip will disappear. The larger the Ω, the larger the rips are and the larger the rip spacing will be (Short, 1985). This is because larger rips are correlated with a lower frequency of rips. The smaller frequency of rips results in the spacing to be subsequently larger (Short, 1985). Erosion rips have velocities of approximately 1 m/s, are usually smaller in width than accretion rips, and cause morphological changes by moving larger amounts of sediment from the foreshore and depositing the sediment beyond the breaker line (Short, 1985).

2.c.1.b Mega Rips

Mega rips are topographically controlled and are relatively large, usually greater than 1 km (MacMahan, Thornton, Reniers, 2006; Short, 1985). In general, the rip is forced by local geology and remains in the same location because the conditions are present to sustain differences in the wave set-up that feed the current (Short, 1985). Mega rips can have velocities that exceed 2 m/s. Short (1985) also describes how mega rips are associated with a beach state that changes from intermediate to fully dissipative. This is due to nearby topography that may prevent the beach state from becoming a fully dissipative state (Short, 1985). The initial rip can occur with $\Omega > 6$, which would be a dissipative beach state (Short, 1985). Even though the Ω would suggest a dissipative beach state it may take between a few days to a few weeks for the beach state to become fully dissipative (Short, 1985); during this time the topography of the area (embayment) will control the rips resulting in a more persistent mega-rip ($\Omega > 6$) (Short, 1985). During this time, the wave conditions would have only changed slightly, resulting in the continued development of mega rips until a fully dissipative state is reached (Short, 1985).

2.c.2 Rip Shape and Nearshore Morphology

Rip current "morphology" can be described as one that has an associated feeder channel that parallels the shoreline usually located in the trough, which collides and

moves through the deep rip channels (MacMahan, Thornton and Reniers, 2006; Wright and Short, 1984). There is a rip neck in which the main current is flowing towards the breakers and a rip head where the current dissipates (MacMahan, Thornton, and Reniers, 2006). The rip channel the current flows through can be incised on a transverse bar or through an alongshore bar (MacMahan, Thornton, and Reniers, 2006). According to MacMahan *et al*. (2005), storms can have a dramatic impact on the rip morphology, such as the shape, width, orientation and frequency. During their experiment, the nearshore started out with well defined rips along with a transverse bar and rip beach state. Following two storm events, the rips moved 50 m down the coast and were reoriented, even though the transverse bar shape remained. The storms eroded and reworked the nearshore bar, causing new channels to be formed and the old ones were filled in, all resulting in the same bar shape with newly oriented rips further down the coast. About 20 days later, a major storm caused erosion of the transverse bar and accretion inside the rip channels decreasing their width and depth. This morphological change could result in a changing beach state and rip current type (Short, 1985).

Brander and Short (2000) found that when the beach state changed from an intermediate state (longshore bar and trough) to another intermediate state (transverse bar and rip), the number of rips in the area doubled and the rip velocity increased. The rip current velocities increased because the rip channels began to infill laterally as the sand bar continued to migrate onshore, which caused the decrease in rip channel size. Given the same current flow but with a smaller width to flow through the rip current increases in velocity (Brander and Short, 2000; Brander and Short, 2001).

2.c.3 Rip Spacing

It has been proposed by Hino (1974), that the maximum rip spacing (y_s) on a given beach can be equal to that of four times the width of the surf zone (x_b). This is because the rip spacing is a function of incident wave height (Hino, 1974). These incident waves at a beach can also result in edge waves, which cause an alternating pattern of large and small wave heights (Hino, 1974; Short, 1985). As a result of the edge waves, rip currents develop at every second antinode, evenly spaced alongshore (Schwartz, 2005).

Short (1985) observed Narrabeen-Collaroy Beach in Aurstraila for total of 270 days (102 with observable rips) to analyze the rip spacing. Using his observations and collected wave data he was able to determine a linear relationship between the dimensionless parameter Ω and mean rip spacing a Narrabeen-Collaroy Beach:

$$\bar{y}_s = 81\Omega + 69$$

where Ω is the dimensionless parameter determined by:

$$\Omega = \frac{H_b}{w_s T}$$

Where H_b is the breaker height, T is the wave period, and w_s is the sediment fall velocity. Importantly, Short (1985), was able to show that as the beach state changed from Ω=2.7 (TBR state) to Ω=4.2 (D state), the daily mean rip spacing increased from 252 m to a maximum spacing of 463 m. Short (1985) also found that higher energy (erosive) wave

conditions resulted in greater rip spacing, while lower wave energy (accreting) caused smaller rip spacing.

Brander and Short (2000) were able to observe the decrease in rip spacing with the increase in rip frequency. At the beginning of their study at Muriwai Beach there were 54 rip currents with an average spacing of 750 m. At the end of the observations the rip frequency increased to 112 and the average rip spacing decreased to 365 m. The increase in frequency of the rips was correlated with the shift in beach state from longshore bar and trough at the beginning of the experiment to a transverse bar and rip and the end. A longshore bar and trough beach state has far fewer instances of possible wave set-up differences than that of a transverse bar and rip state. The longshore bar and trough is one long bar with occasional breaks in the bar which result in wave set –up and rips at larger spacing (Brander and Short, 2000). The transverse bar and rip state results in the bar being attached to the beach at multiple locations. When this happens, the wave set-up is different along multiple locations of the bar and rip currents will occur more frequently at smaller spacing (Brander and Short, 2000).

Thornton, MacMahan, and Sallenger (2007) showed that rip currents develop at the middle of mega-cusps. Mega-cusps are embayments along a beach that develop in a rhythmic pattern (MacMahan *et al*., 2005). These cusps are controlled by edge waves (Guza and Bowen, 1981). This is because cusps facilitate the creation of rips due to their shape. Water is funneled to the center of the cusp where the currents collide forcing the water offshore (rip current).

The difference in all of the controls for rip spacing noted above is that all have a different circumstance in which they are useful. Using the control that the maximum rip spacing is four times the width of the surf zone can be very problematic, because it can be extremely difficult to measure precisely the width of the surf zone (Brander and Short 2000). The linear regression relating the dimensionless parameter Ω to the rip spacing has not been tested on other sites, so it may be a site specific equation. The edge waves and mega-cusp correlation to rip spacing appears to be more accurate. However, the relationship assumes that there is a distinct edge wave presence on a given beach and that there are fully developed mega-cusps. There are not always developed mega-cusps on a beach so the control on rip spacing would only work on the beaches which they do form.

2.d Flow Kinematics

Generally, rip current flow velocity is at its maximum in the middle of the channel and decreases from the middle of the rip channel to the edges of the rip channel (Brander and Short, 2001). Another characteristic of the flow velocity within the rip-neck is that velocity changes with depth within the rip-neck (Brander and Short, 2001). From the bed to the water surface, the flow velocity increases then decreases near the surface (Brander and Short, 2001). This is due to the amount of friction the rip channel puts on the current will decrease as the distance from the channel increases (Brander and Short, 2001). At a certain point, the air will begin to cause friction, resulting in the

current velocity to decrease again as you near the surface of the water (Brander and Short, 2001). There can be a change in the velocities associated with the rip neck and the feeder channels when changes occur to the beach state. As sand bars migrate onshore, the feeder channels may become infilled with sediment resulting in the constriction of the rip channel, causing mean velocity to increase (Brander and Short, 2000; Brander and Short, 2001). However, the mean velocity of the feeder channel may decrease. Even though the feeder channel is flowing at a smaller velocity than before, the decrease is rip channel width may still be enough to constrict the channel to the point that the rip current velocity will increase (Brander and Short 2001). Flow velocity in the rip channel is also influenced by water depth (Brander and Short, 2001). With decreasing water depths, there is an increase in flow velocity of the rip-neck (Brander and Short, 2001). The opposite is true as well, with increasing water depth there is a decrease in flow velocity of the rip-neck (Brander and Short, 2001). Flow velocity in the rip-neck is also characterized by the spatial variability of the flow velocity within the rip-neck.

Brander and Short (2001) found that there can be a pulsation of the rip current velocity related to infragravity waves leading to a velocity changes in the rip-neck either increasing or decreasing between 0.4 and 0.8 ms^{-1}. The standing infragravity waves add to the wave set-up, resulting in periodic pulses of increased current velocity.

Rip current velocities increase or decrease in velocity depending on the tidal elevation (Brander and Short, 2001; MacMahan, Thornton, and Reniers, 2006). A tidal control has also been shown in a number of other studies (Sonu, 1972; Short and Hogan,

1994; Aagaard, Greenwood, and Nielsen, 1997; Brander, 1999; Brander and Short, 2001; and MacMahan *et al*., 2005). Using field measurements during their RIPEX experiment, MacMahan *et al*. (2005) was able to measure these differences in rip current velocities at both high and low tide. Their results showed that at low tide, the velocity of the rip current was generally larger than during high tide. This can be attributed to the decrease in rip current width during low tide and an increase in rip current width at high tide.

An important characteristic of the flow kinematics of a rip current are the wave-current interactions (Haller, Dalrymple, and Svendsen, 2002; MacMahan, Thornton, and Reniers, 2006). Low energy rips tend to have almost no wave-current interaction, an increase in bottom roughness and bed shear stress due to waves moving in a current (Wiberg, 2005). Wave-current interactions can cause an impact on rip velocities and depth (Wiberg, 2005). As a result, the impacts on sediment transport within the nearshore increase with increasing wave-current interaction (Wiberg, 2005). For intermediate energy rips, the wave-current interactions tend to be moderate. High energy rips result in large wave-current interactions and consequently results in a positive feedback increasing the rip velocity (Haller, Dalrymple, and Svendsen, 2002). This is due to the waves occurring within the rip channels increasing the depth of the channel and the rip velocity, much like a tidal elevation change mentioned above.

2.e Remote Sensing

One of the first studies to use remote imagery to interpret and analyze nearshore processes was Holland *et al*. (1997). Holland *et al*. (1997) used video imagery to focus on 3-D nearshore phenomena that are difficult to measure using in situ methods. They were able to use their camera imagery to produce a ten-minute time exposure image that showed the wave breaking patterns at Duck, North Carolina. Time exposure or time-stacked imagery reveal areas of an image where waves are breaking, which will also reveal the nearshore bar morphology because the waves are breaking over the bar. In their image, the lighter tones represented the location of the sand bar, which was submerged (Figure 4). In the image below there is a rhythmic bar and rip morphology. This can be seen in the crescentic shape of the wave breaking pattern over the sand bar. Holland *et al*. (1997) showed that nearshore morphology and beach state can be examined using remote imagery, time-stacking, and rectified images. Holman *et al*. (2006) used four years of Argus video imagery to analyze rip current spacing and persistence. Overall they were able to identify 5, 271 rip channels over the four years of imagery. Their analysis of the imagery revealed that at Palm Beach, Australia there is an average of 6.7 rips, which were spaced at an average of 178 m apart. They also found that the average time of the rip currents was 45.6 days. Holman *et al*. (2006) showed how rip current system resets can be visible in the imagery. Following storms the rip current system would reset, resulting in the destruction of the rip channels and the

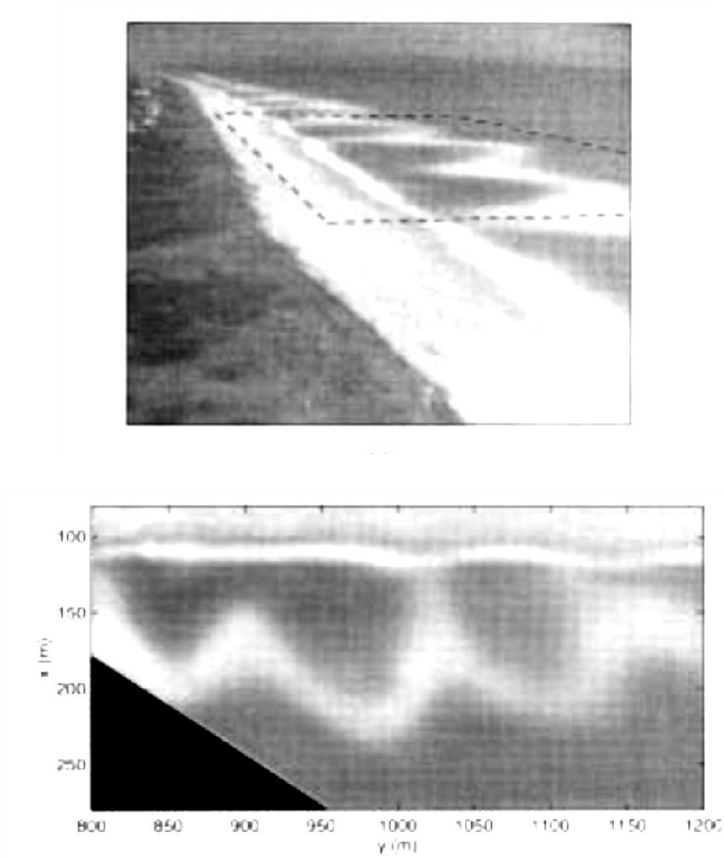

Figure 4: Time stacked wave breaking pattern. From Holland *et al*. (1997). (Top) Image showing the unrectified coastline. (Bottom) Rectified image of the coastline. The lighter regions in the middle showing the breaking wave pattern.

succeeding regeneration of the rip current system. The destruction of the rip channels were hypothesized to be caused by alongshore sediment infilling rip channels during storm events. Similar to this research was that of Aarninkhof *et al*. (2003), who created a video based mapping technique that was used to map intertidal bathymetry. To

achieve accurate mapping they used video imagery to map several shorelines during a tidal cycle. During their research they were able to accurately measure the elevation of a shoreline to within 15 cm over 85% of the region. Video imagery has also been used to examine intertidal beach bathymetry on the monthly and daily temporal scales (Smit *et al*., 2007). Their study was able to predict wave-induced currents by simulating storm conditions over the previously surveyed bathymetry of a specific area. Smit *et al*. (2007) also showed that time lapsed imagery can be used in conjunction with Argus to show how the underlying topography can influence the wave field. The remote imagery was also extremely accurate in locating rip currents and nearshore circulation patterns that were observed in the original video imagery.

Van Enckervort and Ruessink (2003) used remotely sensed imagery taken by cameras to look at how bars behaved along four different sites. The imagery was used to visually analyze the location of the sand bars and the development and destruction of rip currents. They used time stacked images to determine the location of rip channels and of the bars. Their analyses showed that rip currents change between the different beach states and are constantly reworked due to storms moving the sand bars offshore. They used time stacked imagery to show wave breaking patterns in the form of lighter intensity pixels and rip currents as a seaward perturbation that intersects the sand bar. These studies showed that the use of remotely sensed imagery from cameras was effective at studying beach change as well as rip current morphology. Kroon *et al*. (2007) focused on applying remote sensing video systems to coastline management. They used Argus coastal video systems to observe problems prevalent on sandy

coastlines, such as beach erosion, dune erosion, storm related flooding, and anthropogenic impacts (dredging and beach nourishment). Ten minute time averaged video images were used to measure the shoreline position of a beach. Using this as a baseline, they were able to calculate shoreline contours, intertidal beach volumes and changes, the momentary coastline position, and the coastlines response (erosion/accretion) to storm events. The time averaged video images were used to show that the beach slowly recovered in the time following a storm. The time averaged images were also able to show embayments and horns that were altered during the storm failed to recover.

Over the years, new technology and the emergence of remote sensing has resulted in the ability to study the nearshore morphology of a beach in much greater detail. Remote cameras and georectification has given geographers the ability to measure visible and invisible (bar formations) nearshore features with better accuracy and without having to take detailed surveys of the nearshore bathymetry. Remote sensing is now a vital tool in the study of rip currents because of its ability to examine breaking wave patterns.

CHAPTER III

STUDY SITE

3.a Morphology

Pensacola Beach is located on Santa Rosa Island south of Pensacola, Florida (Figure 5). Santa Rosa Island is bounded by the Pensacola Pass on the western end of the island and the East Pass near Destin on the eastern end of the island. Santa Rosa Island is a barrier island which is suspected to have formed in the late Holocene as a direct result of Pleistocene headland eroding near where Grayton Beach is located today (Kwon, 1969). The sediment was transported alongshore following the shape of the coast towards Santa Rosa Island (Kwon, 1969; Stone and Stapor Jr, 1996; Stone *et al*., 1992). The Santa Rosa Island region connects 3 littoral cell systems, the first cell consists of a net alongshore transport of sediment westward from east of the island to the Navarre and Pensacola Beach regions of the island (Stone and Jr, 1996; Stone *et al*., 1992). The second cell has a net alongshore transport of sediment westward from Pensacola Beach to the Pensacola Pass, while the last cell results in a net alongshore sediment transport eastward from Perdido Key to the Pensacola Pass (Stone and Jr, 1996; Stone *et al*., 1992).

A major characteristic of the Santa Rosa Island region is the presence of offshore submarine ridges and swales (Figure 6); (Houser, Hapke, and Hamilton, 2008; Hyne and Goodell, 1967; Stone *et al*., 1992). These ridges and swales have a northwest to

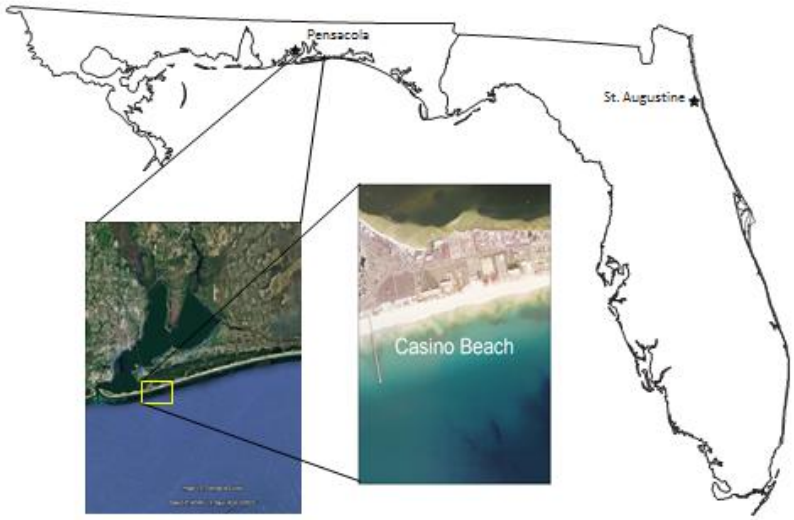

Figure 5: Location of Casino Beach located on Santa Rosa Island in the northwestern part of Florida.

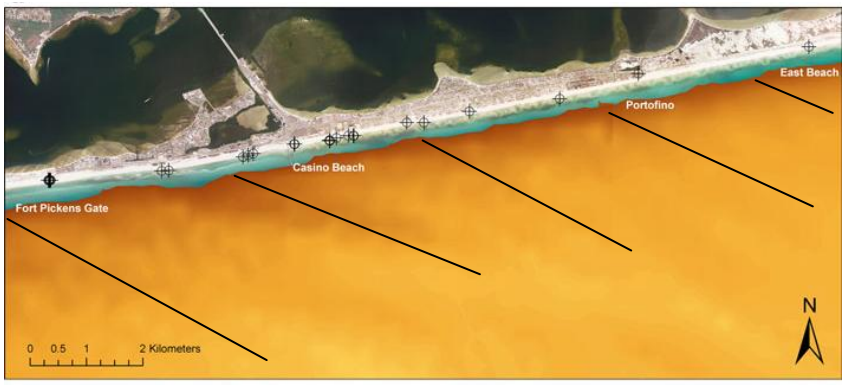

Figure 6: Image showing transverse ridges along with shelf bathymetry along Pensacola Beach. Also the beach drownings between 2000 and 2009 are represented. From Houser, Barrett, and Labude (2011). Black lines represent ridges.

southeast orientation at approximately 65 degrees to the shoreline (Hyne and Goodell, 1967), extending approximately 1700 m offshore (Houser, Hapke, and Hamilton, 2008). The nearshore at Casino Beach is also characterized by a sub-tidal bar. The general morphology related to the sub-tidal bar is influenced by the offshore ridge and swale morphology (Barrett, 2011). Between the transverse ridges is a smaller surf scaling parameter leading to the outermost bar moving closer to shore, thereby forcing the inner bar to move closer to the beach and potentially weld (Houser, Barrett, and Labude, 2011; Houser, Caldwell, and Meyer-Arendt 2011). Where and when the surf similarity parameter decreases towards a reflective state (Ω=1), there would be more rips expected as the beach cycles from longshore bar and trough to a transverse bar and rip state. When the inner bar is forced closer to the shoreline during recovery, the inner bar will go through the beach states mentioned previously from Wright and Short (1984). The beach state will go from longshore bar and trough to rhythmic bar and beach, then transverse bar and rip, and finally to a low-tide terrace. This will increase the probability of rip development, peaking during the transverse bar and rip stage.

The Santa Rosa Island area has been affected recently by 5 major storms in the past decade: Hurricane Ivan, Hurricane Dennis, and Hurricane Katrina in 2004, 2005, and 2005 and most recently by Tropical Storms Claudette and Ida in 2009. These tropical cyclones all had an impact on the beach and dune morphology on the island. Specifically, Hurricanes Ivan, Dennis and Katrina impacted the dune morphology on Santa Rosa Island (Houser and Hamilton, 2009; Houser, Hapke, and Hamilton, 2008). Following Hurricane Ivan, the incipient dunes were destroyed by the storm surge.

However, the majority of discontinuous well developed dunes remained intact (Claudino-Sales, Wang, and Horwitz, 2008). The ridges influenced the hurricane impact by causing an alongshore variation in storm surge as well as overwash gradients. As a result of the refraction by the transverse ridges, there was an alongshore variation in wave height and subsequently breaking wave height (Houser, Caldwell, and Meyer-Arendt, 2011). This resulted in an alongshore difference in the impact on the dune morphology and response to Hurricane Ivan. The areas located near the crest of the transverse ridges experienced larger amounts of shoreline erosion than the areas located at the swale. Historically, the trend has been that larger dunes are located at the wider sections of the island and these sections are correlated with the crest of the transverse ridges. The transverse ridges create a dissipative environment at the shore, which promote dune development. The combination of wave focusing by the transverse ridges and the alongshore variation in breaking wave heights leads to an increase in rip current activity between the transverse ridges.

The influence of the transverse ridges on storm surge and wave breaking has also caused an impact on the bar position. The sand bars located between transverse ridges are consistently closer to the shore, even following storms (Barrett, 2011). Storms can move the sand bar offshore but due to the ridge and swale morphology the sand bar will begin to go through the intermediate beach states faster than the areas located on the ridges.

3.b Safety

Pensacola Beach is a highly populated tourist destination, annually receiving approximately 1.8 million visitors, of which the peak is during July (greater than 400,000 vehicles) and at a minimum in December (approximately 200,000 vehicles) (Houser, Barrett, and Labude, 2011). Pensacola Beach also sees a significant amount of water rescues. From 2004 to 2009 there were approximately 12,000 preventative acts taken by lifeguards along with 633 rescues, as well as 25 drowning between 2000 and 2009, which were rip current related (Houser, Barrett, and Labude, 2011).

Along Pensacola Beach there are a number of significant hot spots for rip current related drownings and rescues. A few of these spots are Fort Pickens Gate, Casino Beach, Portofino, and East Beach (Houser, Barrett, and Labude, 2011). The characteristic that all of these locations have in common is that they are located between the offshore ridges (Houser, Barrett, and Labude, 2011). The majority of drownings which have occurred along the Casino Beach area, have resulted from Casino Beach being one of the most populated beaches along Pensacola Beach.

CHAPTER IV

METHODS

In order to quantify and characterize the development of accretion rips over a year, a remote camera was accessed to capture and download images of the nearshore at Casino Beach every minute. The remote camera is located on the Island Empress Hotel at Casino Beach at the approximate location 487084 N 3355698.69 E (Figure 7).

Figure 7: Image showing the camera location (star) and the approximate field of view of the camera (black rectangle). Numbers are apparent rips in the digital orthophoto (taken 03/17/2004), numbered from left to right.

The camera is set up at an orientation to capture images to the southwest, including the pier. These images were collected for a time frame of one year (September 2009 to September 2010) in order to analyze the variation in the bar and rip morphology over a given year. These images were then time stacked in order to determine the behavior of the rip currents. Adobe Photoshop was used to stack the images in a layer and then take the mean pixel out of that layer (Figure 8), similar to the methods used by Aarninkhof *et al*., 2003; Holland *et al*., 1997; Kroon *et al*., 2007; Smit *et al*., 2007; van Enckervort and Ruessink, 2003. The best images to be examined were the ones taken between 8 am and 9 am and 3 pm and 4 pm, this is due to there being very little glare that was reflecting towards the camera. 30 images were taken from the time period 8 am to 9 am and 3 pm to 4 pm to give 2 time stacked images per day when possible. On days that the camera was not working or only captured part of the time frames of 8 am to 9 am or 3 pm to 4

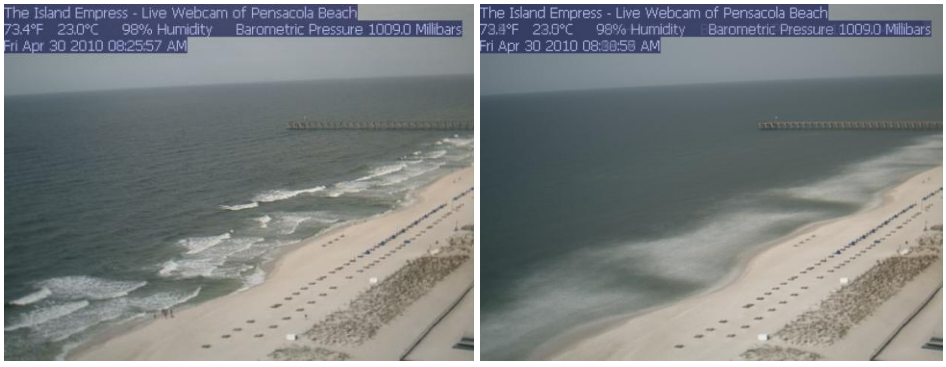

Figure 8: Remote camera image and time stacked image. Image of a single time captured photo (Left). Image of 30 time-stacked photos taken from 8 am to 9 am (Right)

pm, an hour time frame was selected which was the closest to the time that was of interest. Stacked images were created for a total of 200 days of the 365 days of the study. The remaining days were not available for a variety of reasons, mainly due to camera failures or inclement weather obscuring the view of the camera. A total of 21 days occurred in which there were visible rip channels. Of those 21 days, 5 days had rips occur which were visible and captured by the camera at both the morning and afternoon time frames. All other days had one of three other possibilities: 1) no image for the day, 2) a calm nearshore with no visible breaking waves, and 3) large breaking waves, encompassing the entire nearshore.

The reason for stacking images daily is that the accretional rip currents at Pensacola Beach rarely change on short time scales such as minutes and hours like erosional rips. In rough to stormy conditions (large waves, rain), the visibility of the nearshore becomes much less than that of a clear day and almost no rip current activity can be distinguished. The vast majority of change occurs during or after storms as the system is recovering. Specifically, the images will be examined using ArcMap to determine the edges and center of all observable rip channels in order to determine mean width, area, and dominate direction of the rip channels. The rip channel direction and the total number of rips in a given time frame (day, month, or season) were used to determine the mean orientation and frequency of the rip currents.

A rip channel can be identified as a clear discernible gap in the breaking wave pattern (Holland *et al*., 1997; Holman *et al*., 2006; MacMahan *et al*., 2005; Smit *et al*.,

2007; and van Enckevort and Ruessilink, 2003). An example can be seen in the middle of the time stacked image of Figure 8. These images were examined for seasonal variations between the four seasons (winter, spring, summer, and fall) in order to determine if there is a seasonal variation. The seasonal variation was examined because there is a drastic change in weather conditions and storm activity between the seasons. Storm activity and wave heights peaked in the winter, while during the summer storm activity and wave heights were diminished. The time stacked images were then examined in relation to certain environmental conditions (buoy and weather station data) that have been collected for the Pensacola Beach area. This includes wave and wind data such as average wave height, wave period, wave velocity, wind velocity and direction. This helped determine under what environmental conditions the rip channels change morphology.

4.a Rectification

Due to the obliqueness of the images, all images were rectified in order to create a planar view. Since the images were greatly distorted in one direction, any measurements taken using the base image would result in a value highly inaccurate of the true value on the surface. The planar image will result in more highly accurate measurements. The main remote sensing program used for the georectification is the Georeferencing Mountain Photography created by J. G. Corripio (2004). The program is as accurate as that of the DEM used to create it. However, the program assumes that the

users have access to a DEM, ground control points, and camera specifics. The program was originally designed for georeferencing oblique mountain photos, so this is the first real use of the program in a coastal environment. This program coupled with GPS points of Pensacola Beach, survey points taken at Pensacola Beach and along with the use of ArcMap will enable georectification to be performed. The steps used to create the final rectification are provided below.

4.a.1 Collection of GPS Points and Survey Data at Pensacola Beach

The initial step in the rectification process was to collect as many GPS points and survey points as possible inside the field of view of the remote camera. The GPS points were taken using a Garmin GPS Map 60CSx handheld GPS unit and the survey points were compiled using a TOPCON Total Station. The accuracy of the handheld GPS was 3-5 meters. A total of 100 GPS points were taken for the use as possible ground control points in the rectification process. Points were taken at permanent and semi-permanent features located in the field of view of the camera. The main points were large vertical poles in the beach, corner points of the large vegetation areas, end points of a fence, and every post located on the pier that is in the view of the camera. Also, because a majority of the image is the Gulf of Mexico, many GPS points were taken on the beach when the location of the field personnel with the GPS was in the view of the camera. All GPS points can be seen in Figure 9 below. There is only one point between the pier and the

large cluster of GCPs on the right because the area in between was not clearly identifiable on the remote images.

Figure 9: Image showing the location of each GCP taken in the field (Star)

4.a.2 Generation of Files Needed for Input in the Georeferencing of Mountain Photography Program (GMP)

In order for the Georeferencing of Mountain Photography program to work, the files that are inputted must be in a certain format containing various types of information. The DEM and visibility indexes were created using ArcMap and converted into GeoTiff formats using ArcMap. The image to be rectified was saved as a TIF format, which is the correct file type for the program. The GCPs and camera specifics were entered into Microsoft Notepad and saved as standard text file. Once all files are created, Microsoft Notepad was used to create one master file saved as .set, which contains the DEM, Visibility Index, GCPs and camera specifics. The .set file can then be uploaded to the program.

4.a.2.a Creating a Digital Elevation Model (DEM) to be Used in the GMP Program

A DEM of the area in question is needed to successfully rectify an image from the remote camera to a planar view. The remote sensing program requires a DEM that is large enough to show the field of view of the camera. However, the camera location must be location inside of the DEM. To generate a DEM that encompasses the field of view of the camera and the camera, the survey data and a few GPS points are needed.

The survey data was entered into Excel and converted to a UTM coordinate by using an Excel solver. The output of the solver resulted in the survey data being transformed to the UTM coordinate system that the original GPS points were taken in. After this conversion, the heights of the survey data were all changed to 0. This was done because the height changes along the small width of the beach are very minimal and the majority of the image was the surface of the Gulf of Mexico. The new GPS points along with their heights are converted into a feature class using ArcCatalog. The feature class is generated using the same coordinate system that the GPS points were collected using, which was UTM WGS 1984 Zone 16N. This coordinate system was used for all remaining files throughout the course of this project. After the feature class was created, an IDW was generated using the newly created feature class. The 3D Analyst Raster Interpolation tool was used to create the IDW. The generated IDW was used for the DEM to be inputted into the GMP program. The created DEM had a spatial accuracy of within 2.5 m. The accuracy of the elevations were all within a meter, but as stated above all of the heights had to be changed to 0 m because there was almost no change in elevation and the majority of the image was the water surface.

4.a.2.b Creating a Visibility Index to be Used in the GMP Program

An input that was needed for the program was a visibility index. This shows the portion of the DEM that was visible in the image. The Visibility Index needed to be generated had to be in the same format as the DEM and contain the same dimensions.

To accomplish this, the DEM that was created was loaded into ArcMap, then 3D Analyst tool Viewshed, which is located under the Raster Surface tools was used to create a visibility index of the field DEM. Essentially, the Viewshed tool uses an input raster (DEM) and an input observer location and computes the field of view of from that location based off the inputed observer height and angle. To generate the best field of view possible the height of the camera was approximated to be 39 m, with camera angle azimuth being 217. The height of the camera was approximated by determining how many floors/stories the camera was located above the ground by using a building that was visible in the image and estimating how many floors above the ground appeared to be level with the camera. The azimuth was taken from the azimuth given by the GMP program once only the image was loaded into the program.

4.a.2.c Creation of the Camera Specifics and Ground Control Points (GCPs)

To create the required ground control points for the rectification, four GCPs were selected that were as evenly distributed over an image as possible. To get the best rectification possible the GCPs needed to be located across the image. Two GCPs were selected along the beach near the vegetation (one close to the camera and one furthest away from the camera) because points was needed that were visible in all images that did not change position throughout the year. Two points were selected along the pier because it was the most distorted part of the image. Also, the end of the pier point was

chosen because a GCP was needed that extended into the nearshore in order to rectify the image. Only four ground control points were used because that is all the program allows to be used. The UTM coordinates for these four points were then entered into Notepad in order to put them in the format required by the GMP program. To determine the camera specifics that the GMP program requires, the rest of the data was loaded into the GMP program and the target coordinate, focal length, resolution dcpm, film width, film height, offset x, offset y, and camera rotation in degrees were adjusted until the GCPs matched the image as best as possible. The above camera specifics had to be estimated as a result of using a remote camera that was not accessible to obtain the exact camera specifics.

4.a.3 Rectification Using the GMP Program

The files were created and put in the correct format and were loaded in the GMP program. The program was started, which creates a view of the GCPs (Figure 10). The program selects the best four ground control points between the ones entered as well as the target coordinate. The GCPs to be used were then displayed as green crosses which can be seen on the image. The program creates an image that incorporates the DEM and the original image. In this view the DEM is draped over the image. The original image then appears with the DEM superimposed on it (Figure 11). The original image is rectified using the DEM and the ground control points to create an image that appears to be in a planar view. The program created three outputs (Figures 11, 12, 13):

- Original image with the DEM superimposed on it (Figure 11);
- Rectified image in the form of a reflectance map (Figure 12);
- Georeferenced image without the reflectance contours (Figure 13).

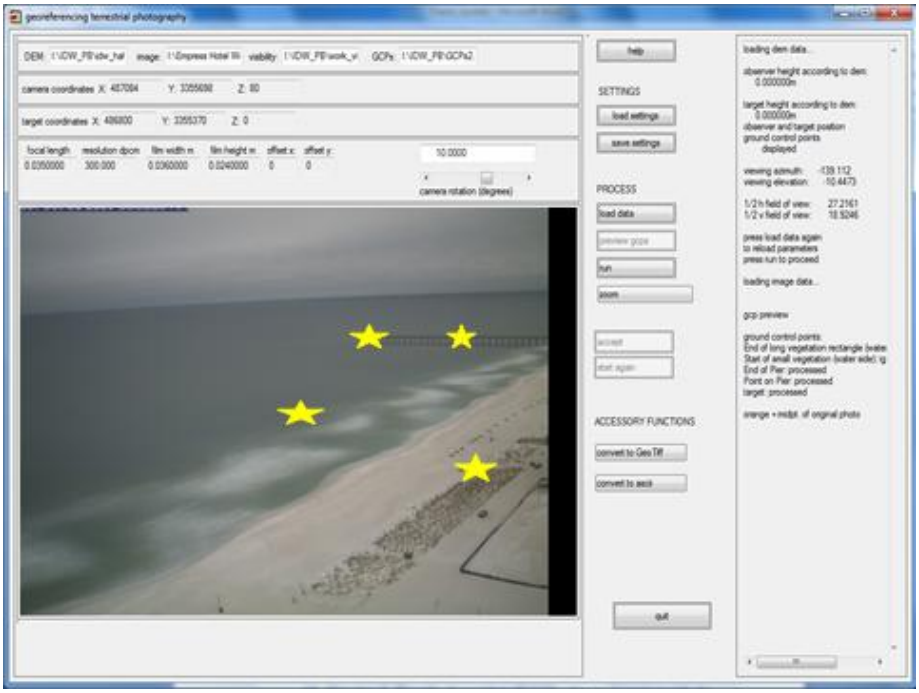

Figure 10: GMP program showing the location of the ground control points and target coordinate (yellow stars).

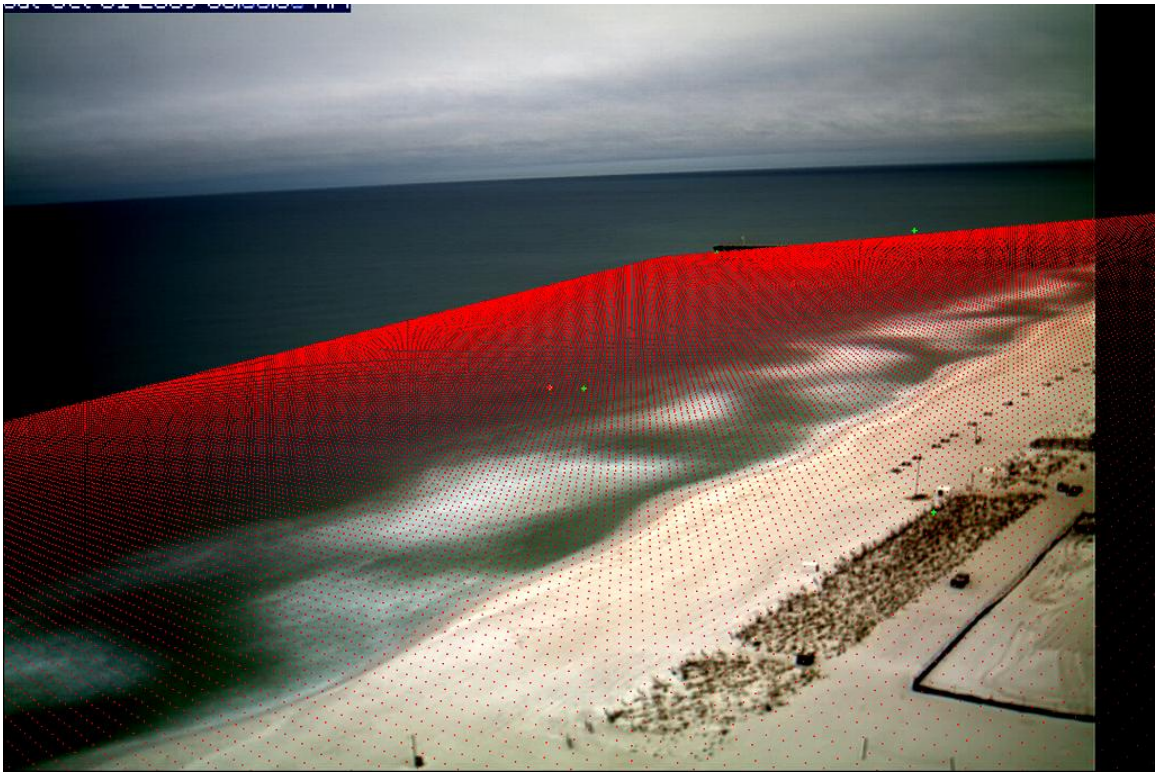

Figure 11: Original stacked image with the DEM superimposed on it. Each red dot corresponds to a cell on the DEM.

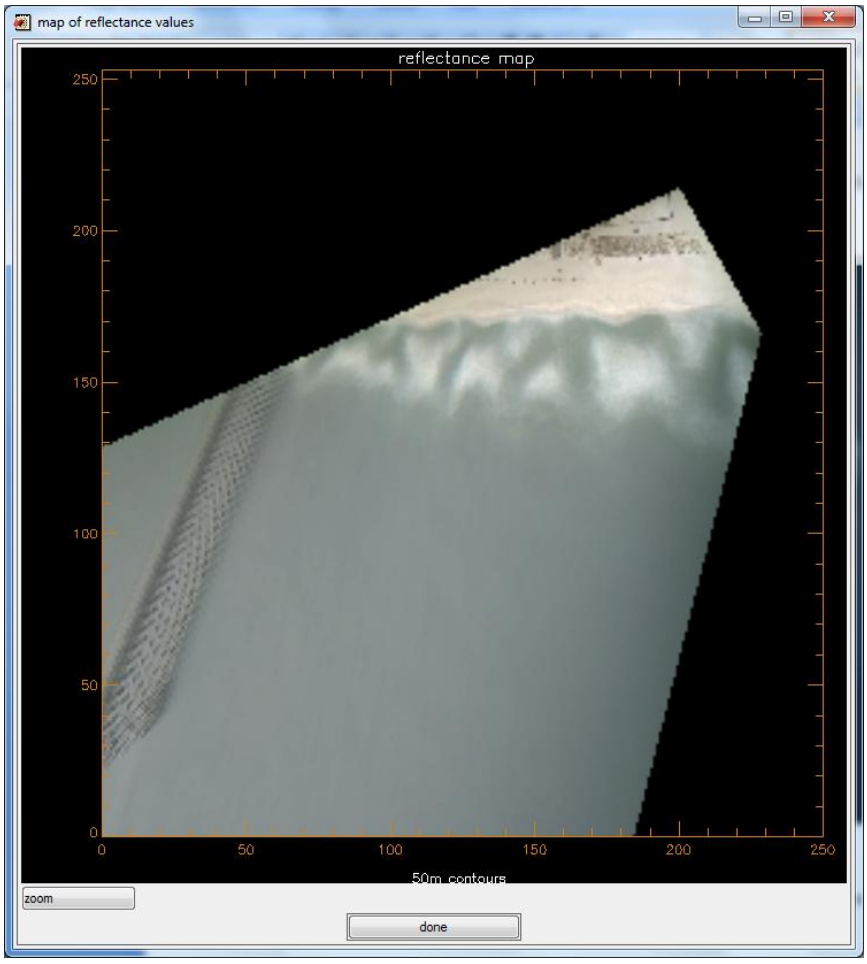

Figure 12: Reflectance Map of the georeferenced image.

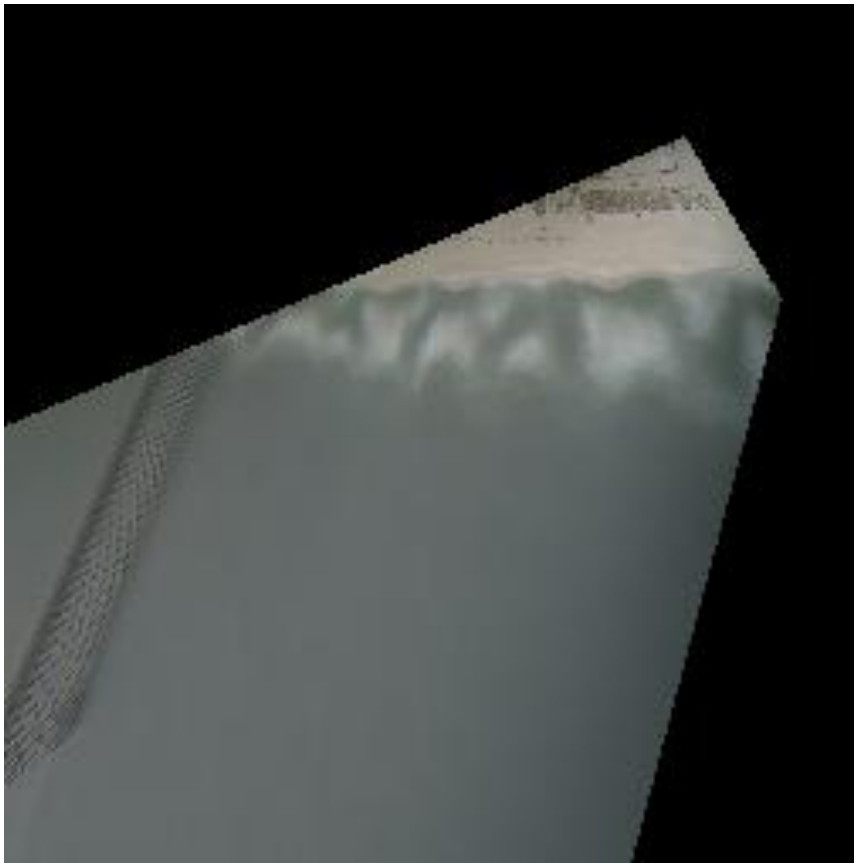

Figure 13: The final georeferenced image without the reflectance contours.

The pier in the above rectification still appears distorted as a result of many factors. One, the pier was the most distorted object in the original images because it was the furthest object away from the camera location. Due to the camera angle being highly oblique, the image gets more distorted as you move away from the camera location. As a result, all of the distortion has not been removed. Two, the pier is the only object that is clearly above sea level. The pier remains distorted because the image was rectified using a DEM assuming all points were at sea level as well as the two GCPs from the top

of the pier. If the pier elevation was used it would have caused the water surface level to be inaccurate because the DEM would show it being above sea level. As a result the pier remains distorted, but the rest of the image is rectified correctly relative to sea level. Basically, there was not enough coverage of GCPs to create a good enough camera model to rectify the pier, which was located in the water.

4.a.4 Determine the Accuracy of the Newly Created Georeferenced Image

Once the georeferenced image has been created, it is essential that the accuracy of this image was to be examined. To examine the accuracy, the newly georeferenced image was superimposed on top of a digital orthophoto taken on March 17, 2004 (http://data.labins.org). The digital orthophoto was of 1 m resolution and encompasses the Gulf Breeze Quad. After looking at the digital orthophoto comared to the georeferenced image it was apparent that there were still some errors with the georeferenced image (Figure 14). The most likely reason for this is because the exact camera specifics were not known for the remote camera. Also, the rectification program was designed for large changes in elevation instead of a mostly consistent elevation.

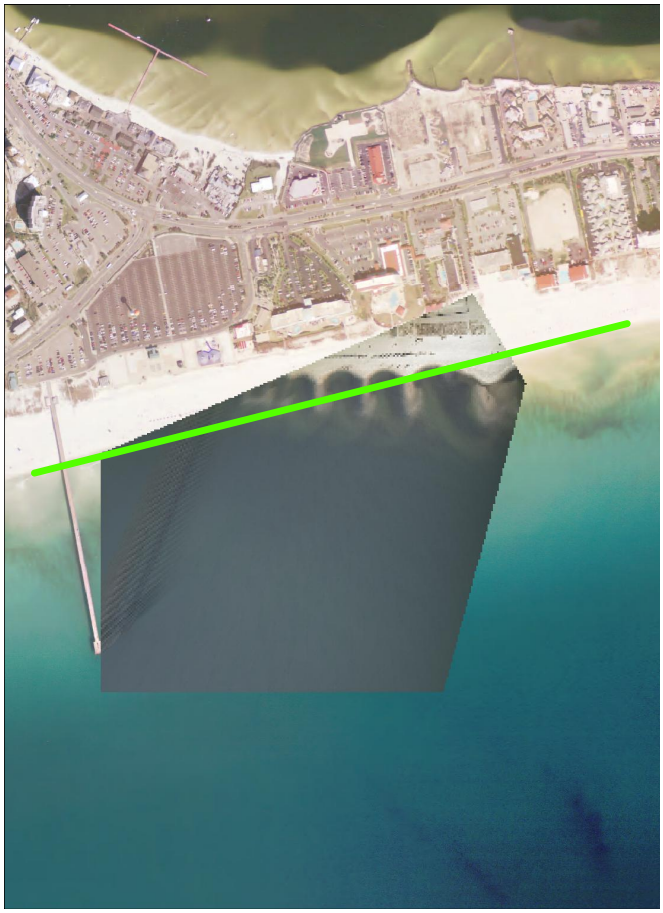

Figure 14: GMP program georeferenced image superimposed on the digital orthophto of the same location. The green line is the end of the beach on the digital orthophoto.

The GMP program rectified the image to a planar view and in the correct coordinate system. However, the image was slightly compressed and at a small angle off of the digital orthophoto. To correct these errors the georeferenced images were georeferenced in ArcMap.

4.a.5 Georeferencing Using ArcMap

As noted the georeferenced image created by the GMP program has a few errors (angle of the image, compression of the image) that needed to be corrected with the georeferencing tool in ArcMap. This process is referred to as rubber sheeting in ArcMap. After loading the original georeferenced image into ArcMap, the GPS locations taken in the field were also loaded into ArcMap. Five ground control points were selected that were the easiest to discern in the image as well as five points that were visible in all successive images (Figure 15). Once the GCPs are selected the image is adjusted in a way that the ground control points on the image match those of the real world as closely as possible. This results in a newly georeferenced image (Figure 16). For the images occurring between September 24, 2009 and February 23, 2010 the RMSE of the ground control points used was 17.32 m. For the images rectified between February 24, 2010 and April 4, 2010 the RMSE was 18.61 m. The two days of April 5 and April 6 of 2010 had a RMSE of 16.45 m. The last set of images between April 7, 2010 and September 24, 2010 had a RMSE of 8.99 m. The reason for multiple sections of images with differing RMSE is because the remote camera shifted slightly throughout the study resulting in slightly different angles of the images.

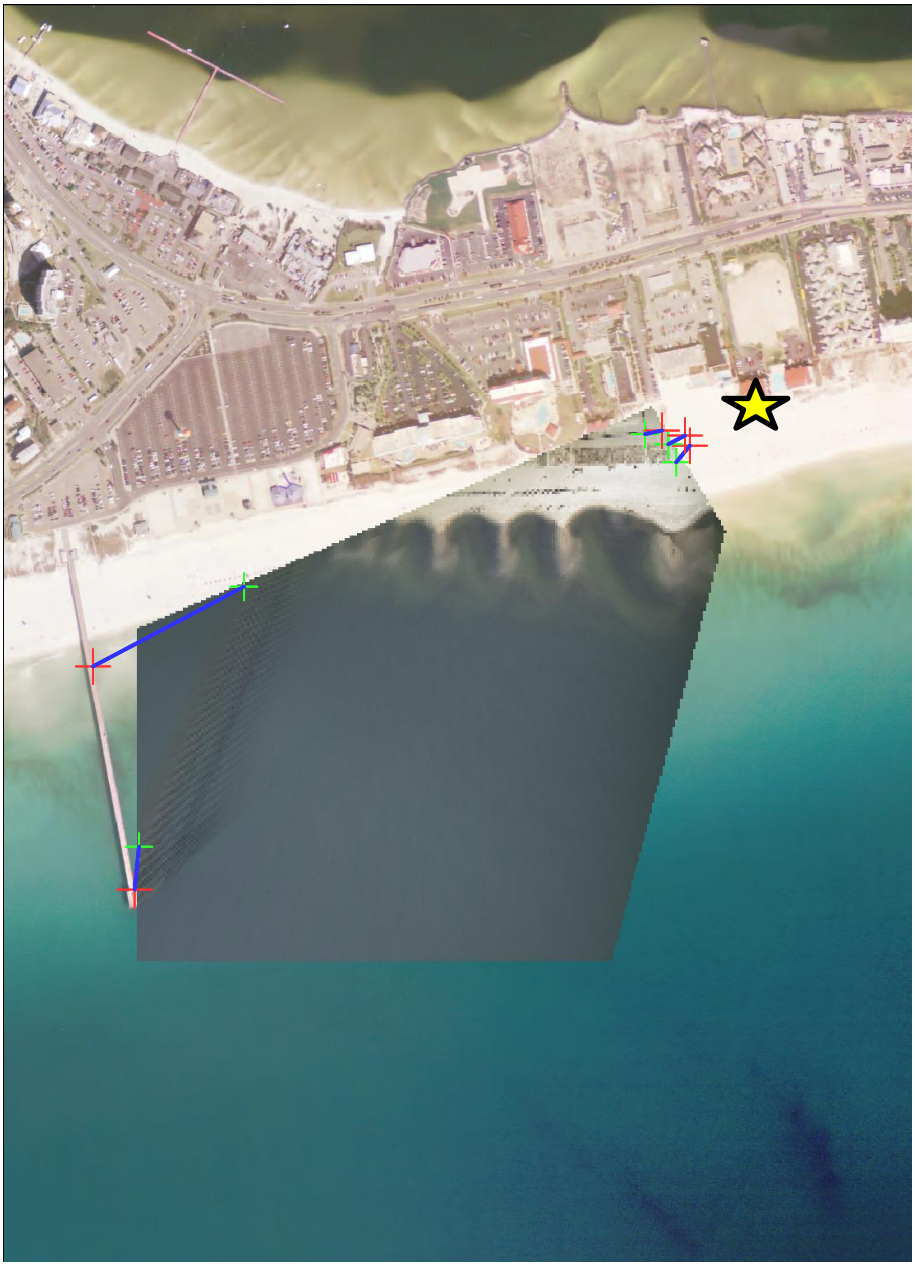

Figure 15: GCPs to be used in the georeferencing process in ArcMap. The red crosses are the GPS point and the green crosses are the location of that point on the image. Location of the camera represent by the star.

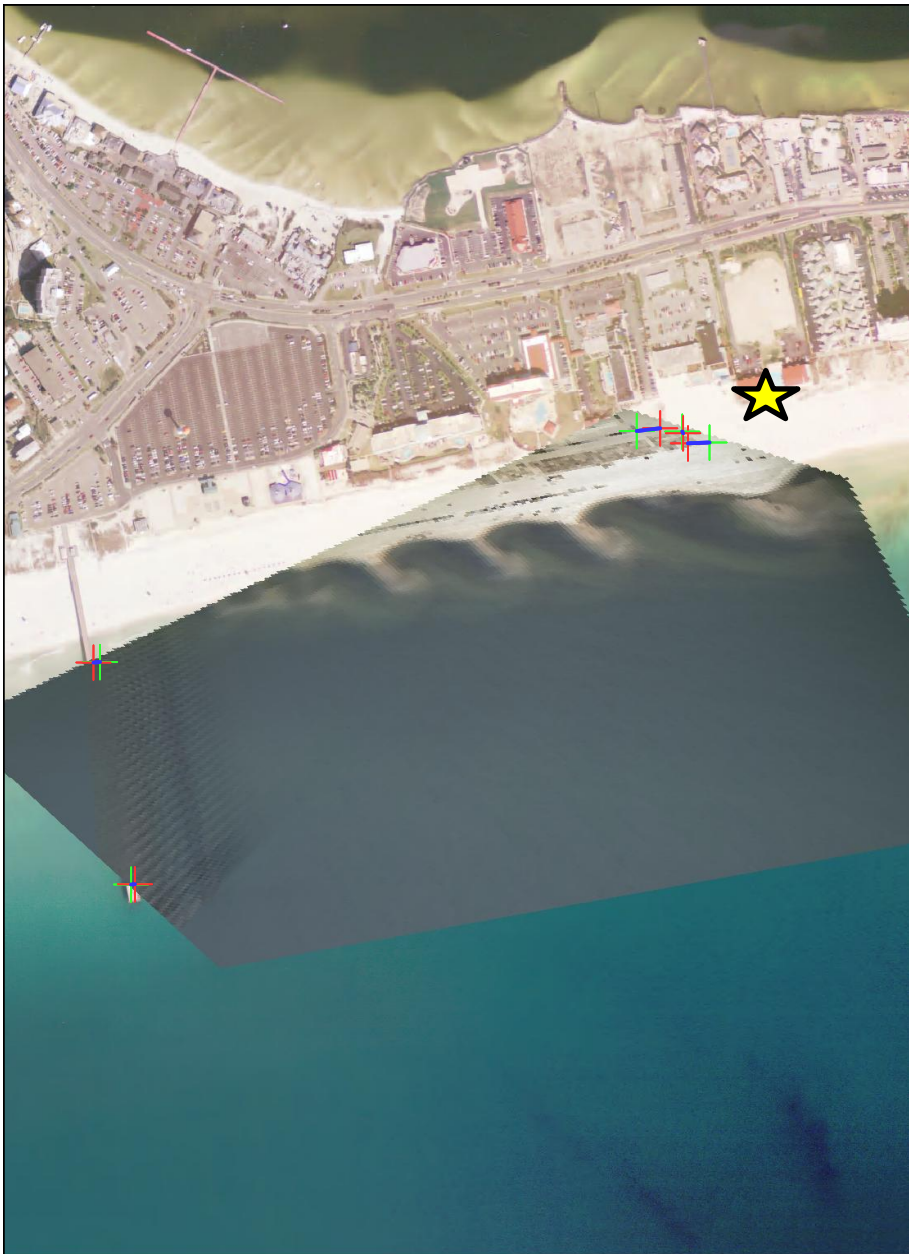

Figure 16: Newly georefereced image superimposed on the digital orthophoto. The red and green crosses are actual locations and the location of the GPS point on the image, respectively. The star represents the approximate camera location.

4.a.6 Looking at the Accuracy of the Final Georeferenced Image

To analyze the accuracy of the newly created georeferenced image the image, was superimposed on the digital orthophto (Figure 17). After looking at the final georeferenced image it is appears more planar than the original georeferenced image. The pier is on the same angle as is the beach. Also the image covers the entire area that it should, unlike the first georeferenced image which was compressed. To obtain a more accurate measure of the georeferenced image the distance from one end of a construction fence was measured to the end point of the long vegetation rectangle. The measurement of the two points came to 16.37 meters. This distance was compared to the GPS points of the same points, which measured a distance of 13.92 meters. The georeferenced image then has an accuracy of ~ 2.45 meters.

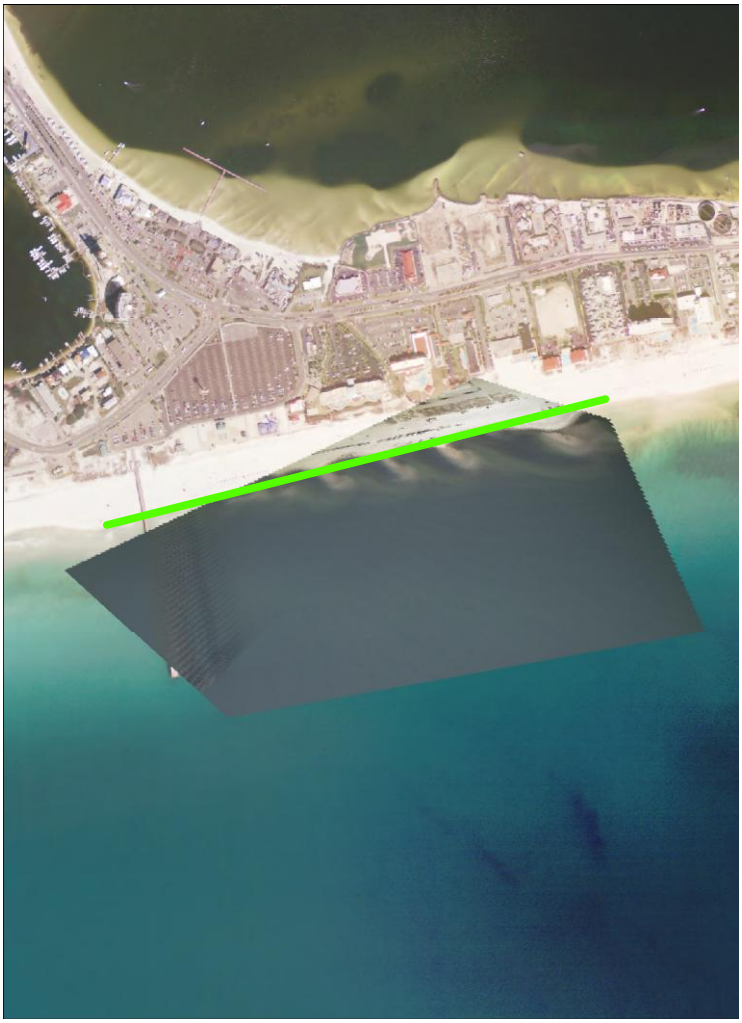

Figure 17: Final georeferenced image superimposed on the digital orthophoto. The green line is the end of the beach on the digital orthophoto.

4.a.7 Georeference All of the Images

The last step in the georeferencing process was to apply all of the previous steps to the rest of the images. As a result of the high volume of images, the georeferencing process was limited to the images that contained rip currents, large storms, or a visible sand bar. For the purpose of this study a large storm was one that cause large frequency of breakers on both the inner and outer bars.

4.b Rip Channel Location

Each georeferenced image was loaded into ArcMap and the center of a visible rip was digitized by a single dot. This location was approximated by eye at the center point where the rip crossed the center of the wave breaking pattern (bar). All discernable rip currents were located in the images spanning September 24, 2009 to September 24, 2010. The center coordinate for each rip was used as the location of the rip. These geographic coordinates were then loaded into excel to create a feature class in ArcCatalog. The rip current locations were then loaded back into ArcMap to create a map of the rip locations.

4.c Rip Channel Angle

To measure the dominate angle of a rip current the georeferenced image was loaded into ArcMap. A line was drawn by hand from the shoreline through the center of the rip current. The center of the rip current was chosen to be the midpoint of the width, which was the most center point of the apparent rip at the intersection of the breaking waves. For rips that contained more than one direction or was highly curved the angle that best encompassed that rip was used. An example of the angle can be seen in Figure 18. Due to the images being georeferenced the angle drawn can be examined using a 360 degree circle to determine the true azimuth of the rip current. For this study 0 degrees represented north, 90 degrees east, 180 degrees south, and 270 degrees represented west. For complex rip shapes, the angle was taken where the rip passed the middle of the wave breaking pattern (Figure 19).

Figure 18: Image showing the dominate angle (black line) of a rip current.

4.d Rip Channel Width

To measure the width of each rip current, each georeferenced image that contained at least one rip channel was loaded into ArcMap. The width of a rip channel was measured from one edge of the rip current to the other edge of the rip current. The edge of a rip current was deemed to be the point where the water pixel changed from dark to a brighter shade or white. This transition was determined to be where the pixel

changed from dark to bright. This measurement was taken as close to the center of the bar/breaking waves as possible, approximated by eyeballing the center of the wave breaking patterns width (Figure 19). Also, this width was taken at an angle 90° to the angle of the alongshore. The same method was applied to measure all rip currents found in each image over the year.

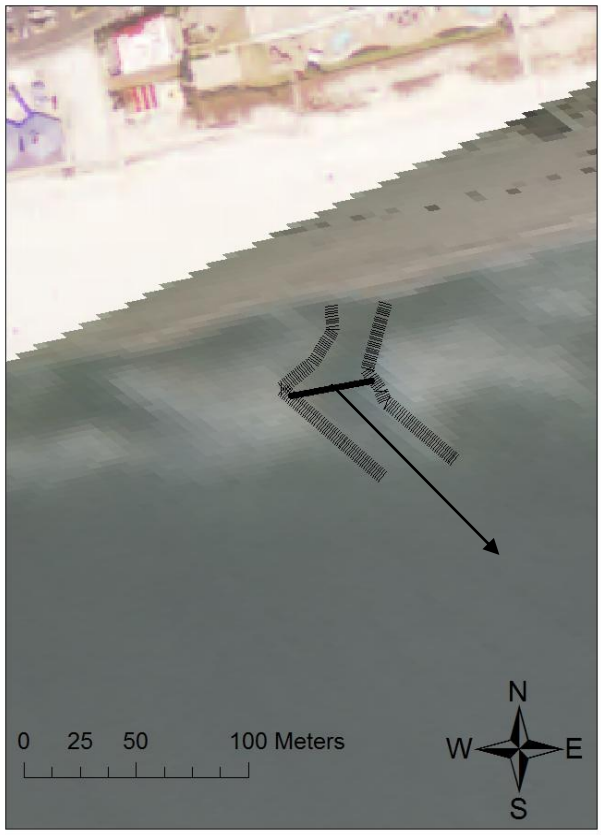

Figure 19: Image of a rip current showing how width was measured. Width of the rip shown by the black line. Edge of rip represented by hashed line. Arrow shows the dominate angle of the rip.

4.e Rip Clustering

To examine the possible clustering of rip currents over the spatial extent of the study site, a combination of S+ and ArcMap were used. An agglomerative hierarchal cluster analysis was performed using the UTM coordinates of each rip current, which resulted in a cluster tree (Figure 20). From there an appropriate and acceptable level was selected and the locations of the rips were assigned to the cluster in which they fell into. The appropriate level for this study was selected to be approximately 50. This level was selected because it resulted in the clusters having a fairly consistent level in similarity (height). On the dendrogram a height of 1 shows the most similarity between the objects (rips) while a similarity (height) of 300 represents the least amount of similarity between the objects in the given cluster. A similarity (height) of approximately 50 was appropriate for this study because the outcome was clusters that were more highly similar within each cluster, but still maintained a large enough difference to have multiple clusters. The circles on Figure 20 show where the selected clusters would be located in the cluster tree at an approximate height of 50.

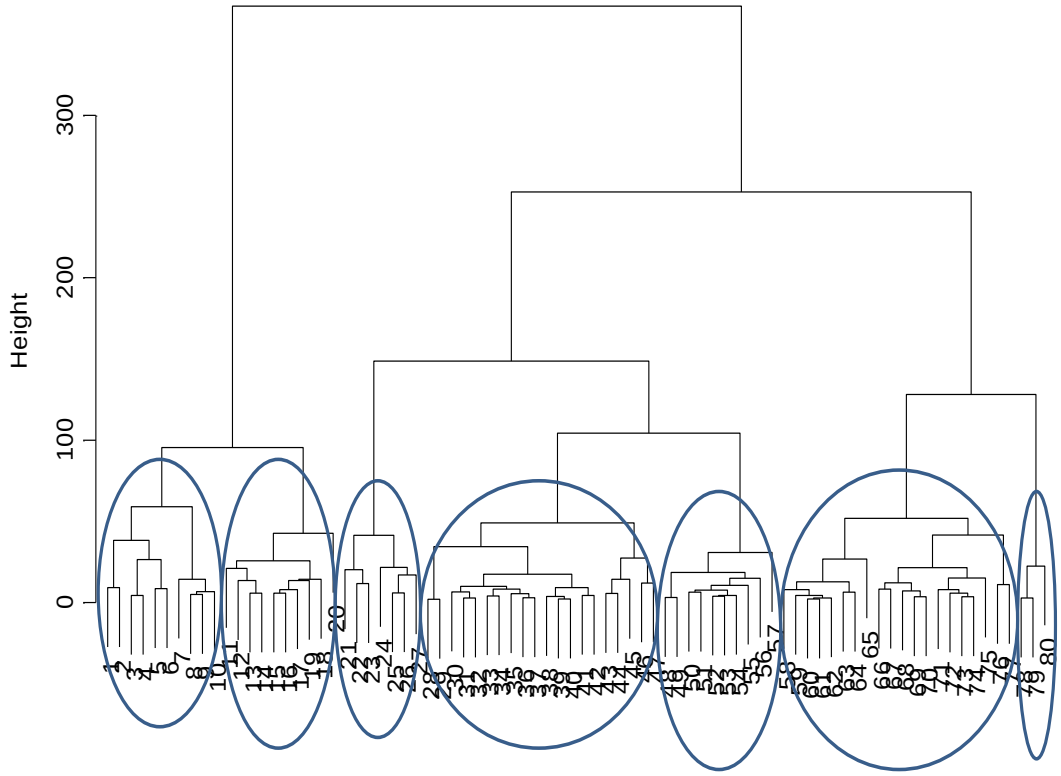

Figure 20: Cluster tree generated using S+. Circles represents where clusters would be at the selected height of 50.

4.f Conditions Resulting in Rips

To obtain a variation in rip hazard over the year time frame (September 2009-September 2010), a combination of the rip morphology (rip width, angle, frequency) were examined in relation to the wind and wave data collected. The rip morphology characteristics were compared to the wave and wind characteristics to determine whether

there was a correlation or pattern that can be seen over the course of the year or between seasons. These were examined in order to obtain the overall picture of the location of the rips, when they occur, and under what conditions they occur. To determine the wave conditions under which rip currents developed, wave data came from NOAA buoy 42012, which is located at 30.065° N and 87.555° W (Figure 21). This buoy is located approximately 31 miles to the southwest of the study site at Casino Beach. From this buoy the significant wave height was used as a proxy for the wave heights on each day of the time frame in question. The buoy data spans from September 2009 to September 2010. However, the buoy data was missing days from September 26, 2009 to October 28, 2009. As a result of the missing data, NOAA buoy 42039 was used to supplement the days that were not captured by the original buoy. Buoy 42039 is located at 28.791 N 86.008 W and is located approximately 126 miles from the study site at Casino Beach (Figure 21). The wave heights used are the significant wave heights computed for each hour. This was calculated by using the mean of the largest one-third of wave heights over a twenty minute section. The wave heights were examined to determine the characteristics of the wave field between rip currents. The wave heights will be compared to the rip morphology characteristics in order to determine if there are any discernible patterns. Specifically, the minimum wave height, maximum wave height, standard deviation of the wave height, and mean wave height will be calculated for each time frame between days with rip currents. The wave angles to be used are the mean direction at the dominant wave period. The wave heights offshore are not an exact representation of the breaking wave heights in the nearshore. The breaking wave heights

at Pensacola Beach are typically within 0.5 m of the offshore height. Another reason for using the offshore wave heights is that previous literature has used them in the calculation of surf similarity parameter. In order to keep the values consistent the offshore wave heights were used in the calculation of the surf similarity parameters and in determining the mean conditions under which reset storms and rip channels occurred.

The wind data came from a weather station located at Pensacola, Florida (Figure 21). The wind speed and direction will be plotted against the significant wave heights to determine the conditions for a given day. The wind angle and direction will be used to determine the conditions which rip currents actually occurred under.

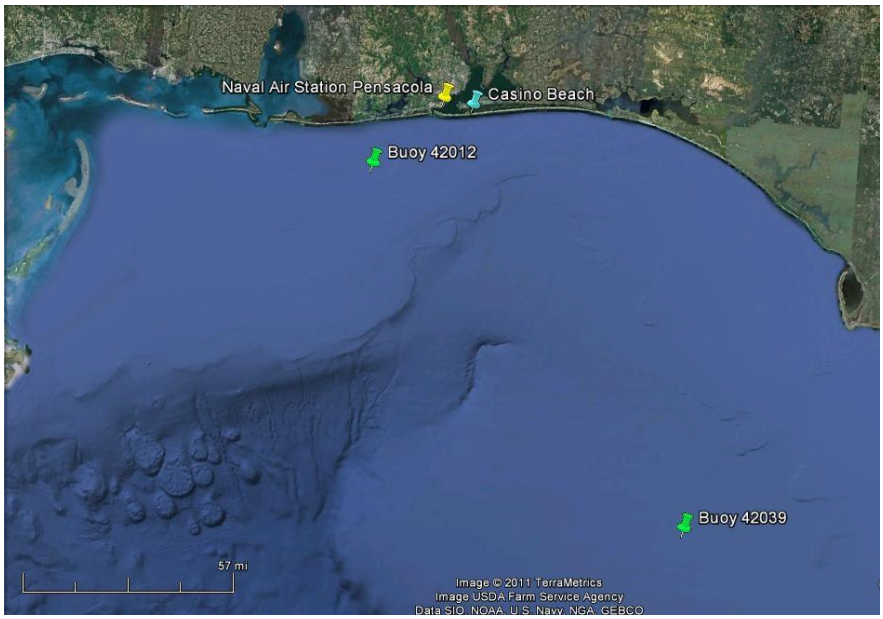

Figure 21: Image showing the location of both buoys used for wave data and the location of the weather station used for the wind data.

CHAPTER V

RESULTS

5.a Rip Frequency and Reset Storms

Casino Beach was dominated by three beach states throughout the study, these were longhshore bar and trough (Figure 22), rhythmic bar and beach (Figure 23), and transverse bar and rip (Figure 24). Of these three beach states the most frequent was the transverse bar and rip state, with the least frequent being the longshore bar and trough state. Also the frequency of rips was maximized as the beach state resembled that of a transverse bar and rip and decreased as it formed into a longshore bar and trough.

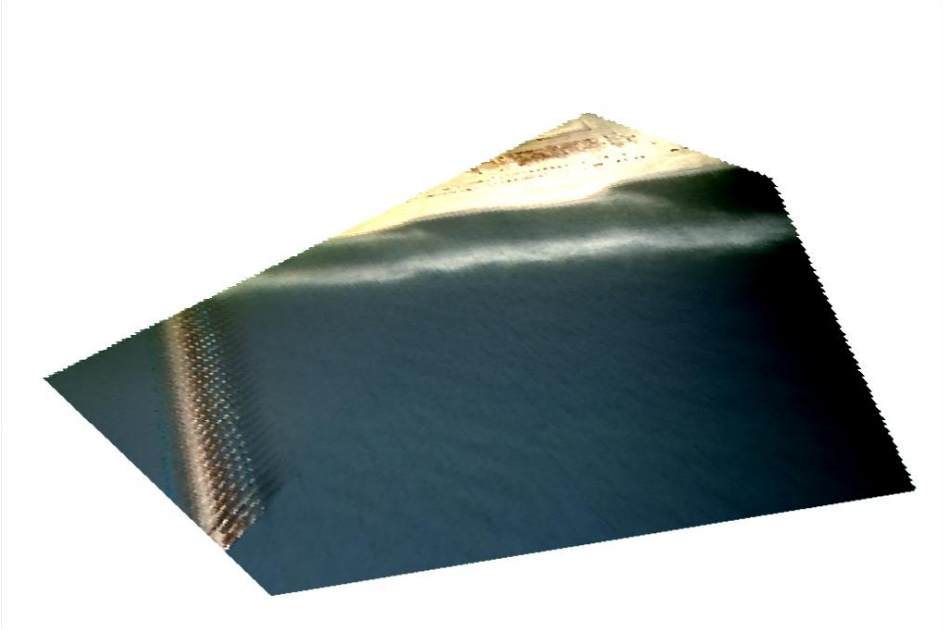

Figure 22: Longshore Bar and Trough

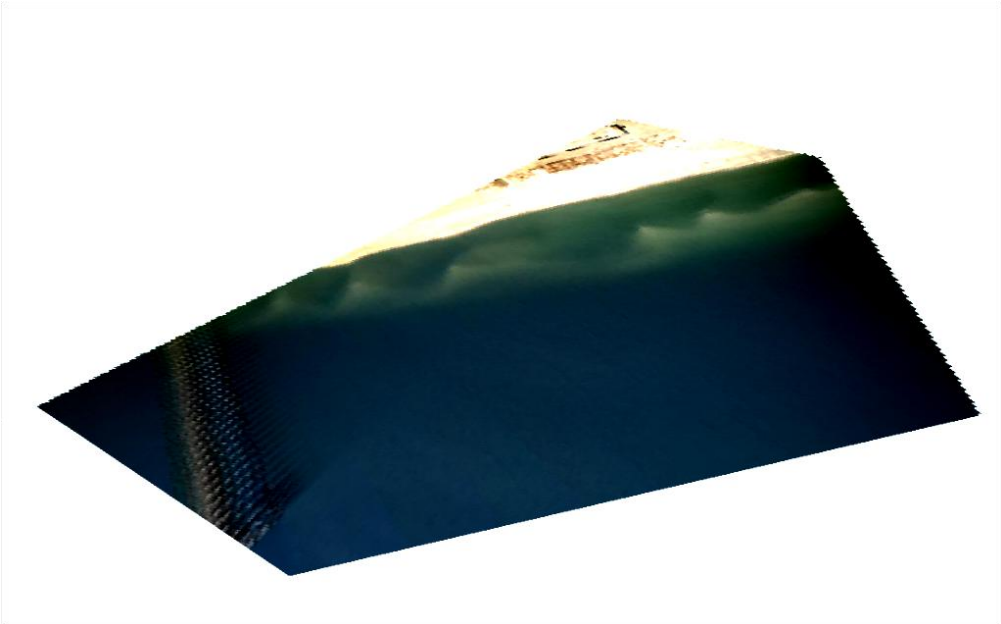

Figure 23: Rhythmic Bar and Beach

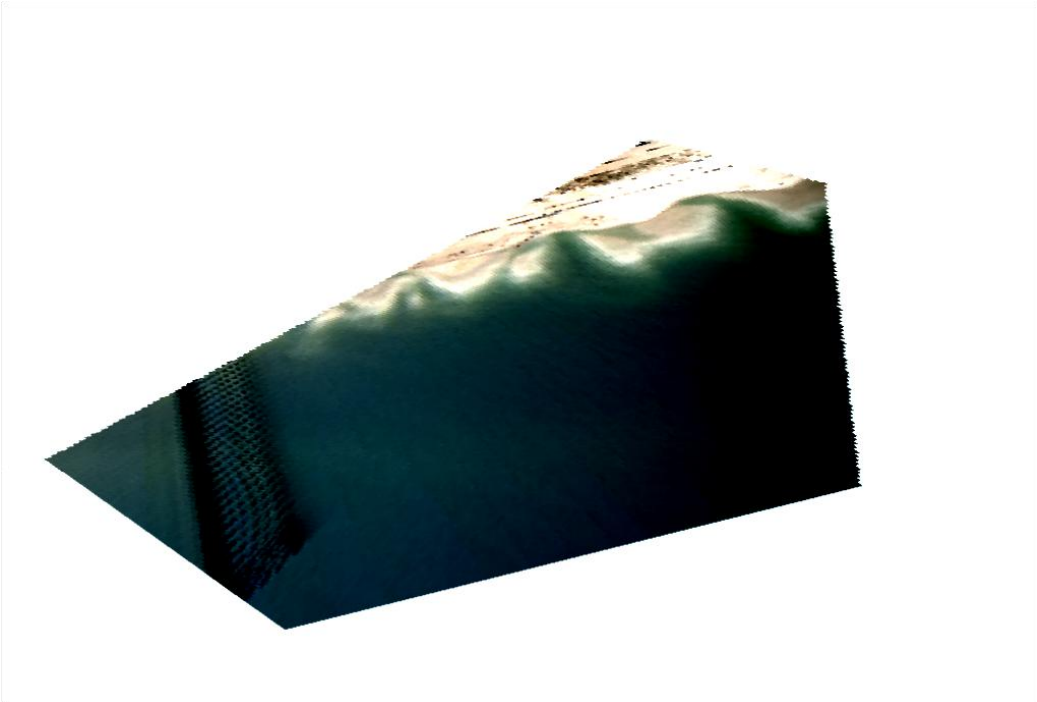

Figure 24: Transverse Bar and Rip

There were a total of 89 rip channels between September 24, 2009 and September 24, 2010 all of which can be classified as accretion rips. Each rip channel visible in a given image was classified as a new rip channel. These rip channels were spread out over 5 months: October 2009, January 2010, April 2010, May 2010, and July 2010. The majority of the rip channels (64) occurred between April and May, 2010. The breakdown of the month by month rip frequency can be seen in Figure 25. At the start of the study, there were zero rip channels (reflective beach state) between September 24 and September 30. For the month of October there were a total of 8 rip channels, which occurred during the month, all of which transpired on October 31. Over the next two months (November and December) there were multiple storms. However, there was no rip channel activity that was visible in the imagery. The sand bar was moved offshore by each subsequent storms not allowing for beach recovery (Figure 26). In the month of January there were 12 rip channels, which occurred on the days of January 17, 22, 25, and 29. All of which contained 3 rip channels per day and occurred in a longshore bar and trough beach state. Again in February and March there were multiple storms and no rip channel activity. The bar was again moved offshore and reset as another longhsore bar and trough morphology.

The highest frequency of rip channels occurred in April and May. During April, 43 rip channels were visible in the stacked imagery. These rip channels occurred on April 5 (6 rips in morning, 5 rips in afternoon), April 7 (2 rips), April 11 (7 rips), April 13 (6 rips), April 14 (5 rips in morning, 3 rips in afternoon), April 27 (6 rips), and April

30 (1 rip). In May, 22 rip channels occurred, which were visible in the obtained imagery. The rips occurred on May 4, 5, 10, 11, 12, 14, 15, and 17. There were 2 rips for each one of the days with May 5, 10, and 17 having 2 rips each in the morning and afternoon. At the beginning of April there was a longshore bar and trough morphology that changed to a rhythmic bar and beach, and finally to a transverse bar and rip morphology towards the end of April. In the months of June, July, August, and September there were only 5 rips, which all occurred on July 13 while still at a transverse bar and rip morphology. Sample images from each month can be seen in Figure 26. As shown in Figure 26, there were 6 months in which zero rip channel activity was visible in the obtained images. There were a lot of factors that influenced this outcome. First, the camera used was not able to capture an image for every day of every month, meaning the days not captured by the camera could have contained rip channel activity. Second, for much of the winter months, frontal storms caused large enough waves that rip current activity might have been obscured in the time stacked images. Because the images are time-stacked, flash rips may have developed but were not visible because large waves may have occurred before or following the rip. This could have resulted in the imagery showing large continuous waves instead of the rip channel. Other than these factors, there was no visible rip activity in the observed images (Figure 26: September, November, December, February, March, June, August) during the 7 months that were recorded as having zero rips.

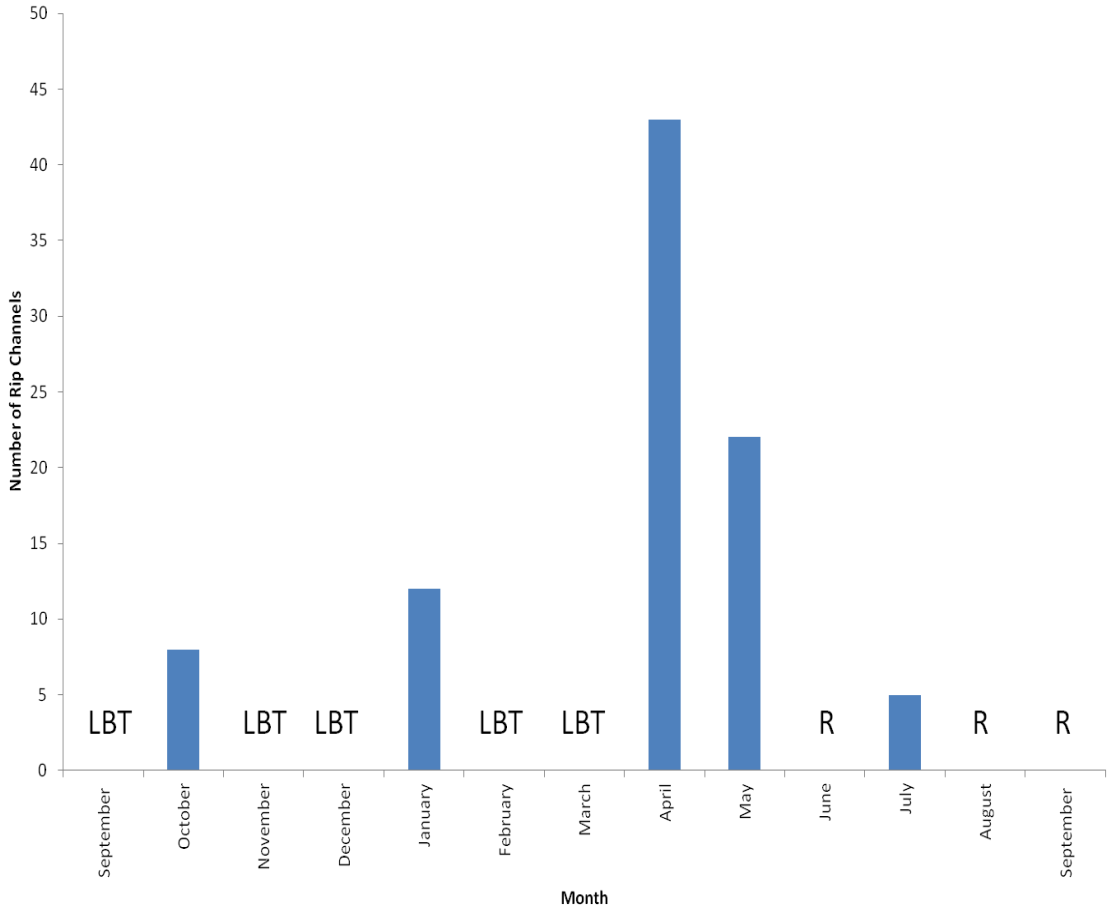

Figure 25: Timeseries showing the rip frequency observed for each month from September 2009 to September 2010. With beach states for non rip channel months (LBT or R)

A) September 2009

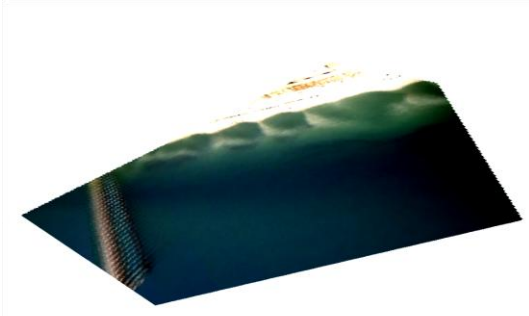

Transverse Bar and Rip

B) October 2009

Transverse Bar and Rip

C) November 2009

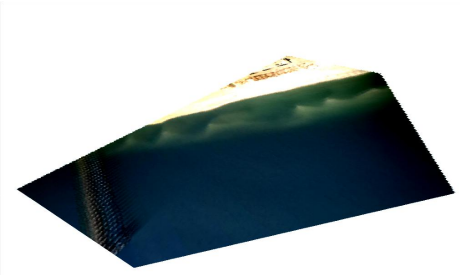

Rhythmic Bar and Beach

D) December 2009

Rhythmic Bar and Beach

E) January 2010

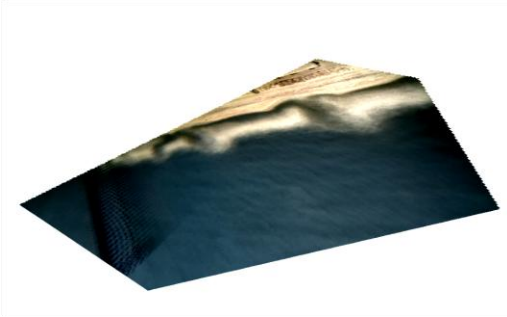

Rhythmic Bar and Beach

F) February 2010

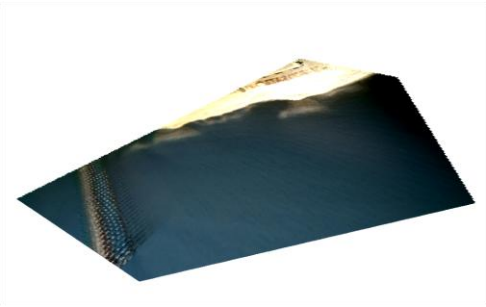

Longshore Bar and Trough

Figure 26: Sample images from each month of the study. Observed beach state listed below each image.

G) March 2010

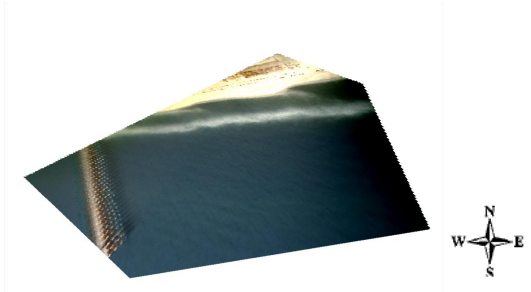

Longshore Bar and Trough

H) April 2010

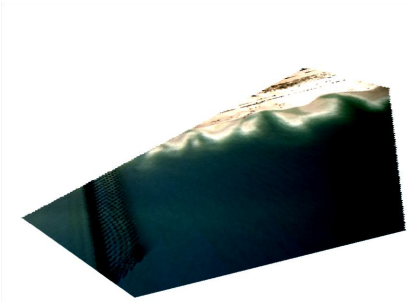

Transverse Bar and Rip

I) May 2010

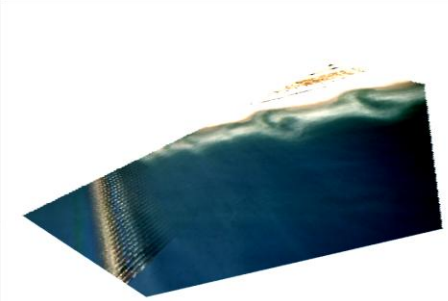

Transverse Bar and Rip

J) June 2010

Reflective

K) July 2010

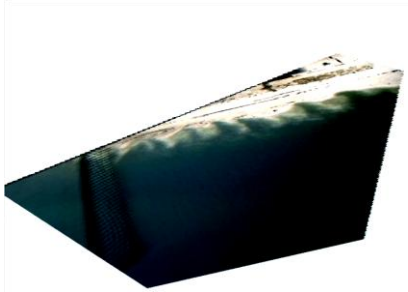

Transverse Bar and Rip

L) August 2010

Longshore Bar and Trough

Figure 26 Continued.

M) September 2010-LBT

Figure 26 Continued.

The seasonal breakdown of rip frequencies can be seen in Table 1. It is important to note that 77 percent of the rips occurred between the spring and summer months. This is important because the majority of beach goers and tourist visit during the spring and summer months leading to larger amounts of people that could be at risk due to the occurring rips.

Table 1: Seasonal breakdown of rip frequencies

Season	Rip Frequency
Fall (S, O, N)	8
Winter (D, J, F)	12
Spring (M, A, M)	64
Summer (J, J, Aug)	5

Over the course of the study, there were a total of 9 reset storms. As noted, a reset storm is any storm events that causes the destruction and subsequent regeneration of the sand bar and rip channels (Figure 27). The destruction and regeneration of the sand bar can be defined as a change in the location, shape, or size of the sand bar following a storm event. The majority of the storm events at Pensacola Beach that reset the bar were not powerful enough to change the beach state all the way to longshore bar and trough. The most powerful (Saffir-Simpson Scale) reset storm occurred on November 10, 2009, which was caused by Tropical Storm Ida that made landfall near Dauphin Island, Alabama with wind speed at approximately 45 mph (Figure 27). The most common storm reset was one that caused the sand bar to reconfigure or move offshore enough to notice a significant change in the position and shape of both the rip channels and sand bar. The average reset storm could also be defined as one which resulted in an average wave height of 2.35 m. Figure 27 shows an example of two reset storms that caused the sand bar to reconfigure also resulting in a change in beach state. The images associated with the November 10 reset storm suggests that the beach state prior to the storm was a transverse bar and rip and the beach state following was that of a rhythmic bar and beach. Similar to the mentioned reset storm above, are the images depicted along with the reset storm on January 17, 2010. Prior to the reset storm the beach state was a rhythmic bar and beach and then following the storm it was in a longhsore bar and trough morphology. The rest of the beach states before and after reset storms can be seen in Table 2. Four of the nine reset storms resulted in a beach state change where the

A) October 31, 2009: Transverse Bar and Rip

B) December 28, 2009: Rhythmic Bar and Beach

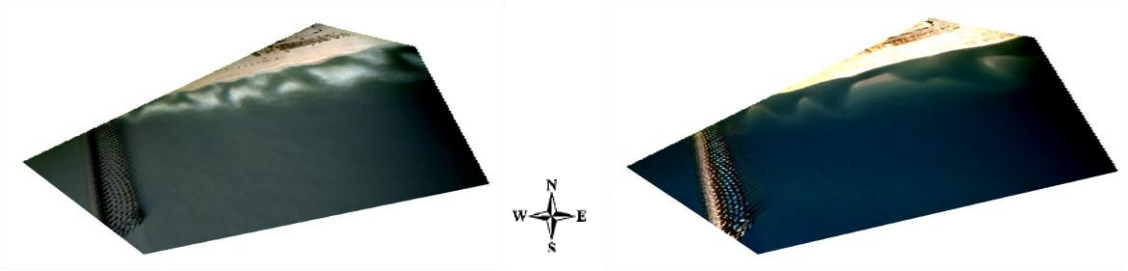

C) November, 10, 2009: Tropical Storm Ida

D) January 16, 2010: Frontal Storm

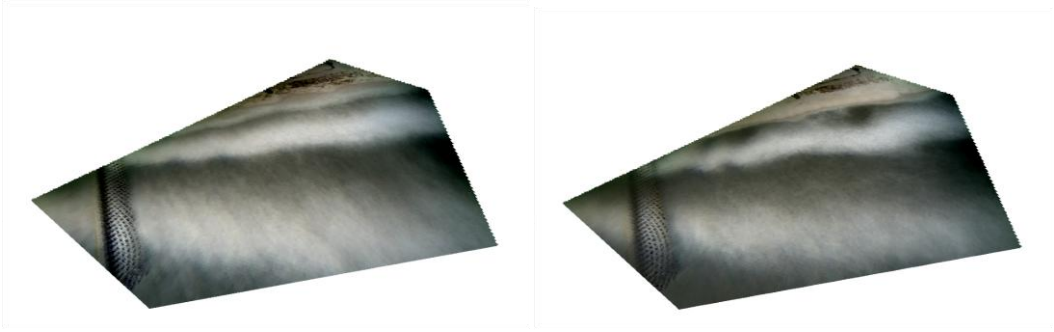

E) November 26, 2009: Rhythmic Bar and Beach

D) January 22, 2010: Longshore Bar and Trough

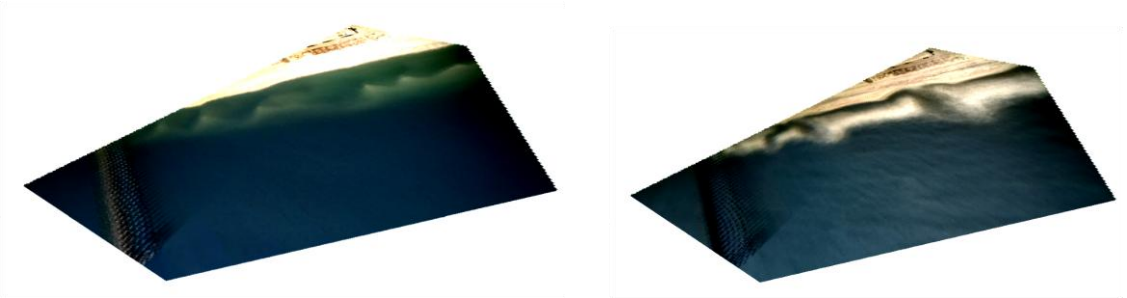

Figure 27: Non-typical (Top Left-Tropical Storm Ida) and typical (Top Right) storm resets seen throughout the study.

bar moved from closer to shore to further offshore (e.g. transverse bar and rip to rhythmic bar and beach). Four of the nine reset storms caused no observable change in beach state, while 1 reset storm resulted in the observed beach change with bar migration onshore (e.g. longshore bar and trough to a rhythmic bar and beach).

Table 2: Observed beach states prior to and after reset storm. Along with the total of recovery days following the reset storm

Reset Storm	Observed Beach State Prior	Observed Beach State After	Total Days Before Next Reset Storm
10/23/09	Transverse Bar and Rip	Rhythmic Bar and Beach	17
11/10/09	Transverse Bar and Rip	Rhythmic Bar and Beach	21
12/2/09	Rhythmic Bar and Beach	Longshore Bar and Trough	15
12/18/09	Longshore Bar and Trough	Longshore Bar and Trough	5
12/24/09	Longshore Bar and Trough	Rhythmic Bar and Beach	22
1/16/10	Rhythmic Bar and Beach	Longshore Bar and Trough	19
2/5/10	Rhythmic Bar and Beach	Rhythmic Bar and Beach	27
3/2/10	Rhythmic Bar and Beach	Rhythmic Bar and Beach	8
3/11/10	Rhythmic Bar and Beach	Rhythmic Bar and Beach	

Between the observed 9 reset storms the conditions were such that the nearshore bar migrated onshore following the Wright and Short (1984) intermediate beach state model. Following a reset storm the bar and rip morphology resembled that of a longshore bar and trough (Figure 28). Two weeks following the longshore bar and trough morphology and after continued bar migration, there was a rhythmic bar and beach morphology (Figure 29). The bar continued to migrate onshore, and after 20 days

there was a clearly visible transverse bar and rip morphology (Figure 30). These three beach states were the primary beach states throughout the yearlong study. The average recovery time between reset storms was 17 days, with the longest time being 27 days and the smallest time was 5 days. The one instance of full recovery occurred between the reset storm on March 11, 2010 and May 26, 2010. Following the reset storm on March 11, the beach state was a rhythmic bar and beach. The bar continued to migrate onshore and recover up to May 26 when the bar appeared to have attached to the shoreline. There were a total of 75 days between the reset storm and the observed reflective beach state. During those 75 days the bar continued to migrate onshore and recover without being interrupted by any reset storms.

Associated with the bar migration onshore was the development of rip channels. A comparison of reset storms and rip channel groups (temporal) can be seen in Figure 31. Before the first group of rip channel group on October 31, 2009, 8 days had passed since the last reset storm on October 24, 2009. 4 reset storms occurred before the next group of rips. These reset storms came on November 10, 2009, December 2. 2009, December 18, 2009, and December 24, 2004. The last reset storm coming 21 days before the second group of rip channels, which occurred on January 15, 2010. The third group of rips (between January 22, 2010 and January 29, 2010) resulted 6 days following a reset storm on January 16, 2010. The final group of rips (between April 5, 2010 and July 13, 2010) occurred following 3 more reset storms on February 5, 2010, March 2, 2010, and March 11, 2010. The last group of rips resulted 25 days following the storm reset on March 11, 2010.

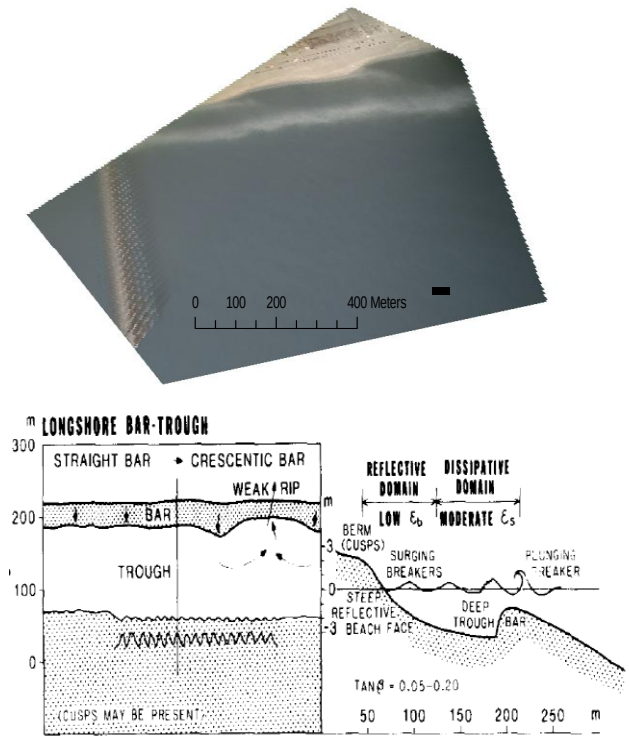

Figure 28: (Top) Image is from March 25, 2010, showing LBT morphology. (Bottom) image was from Wright and Short (1984) depicting LBT morphology

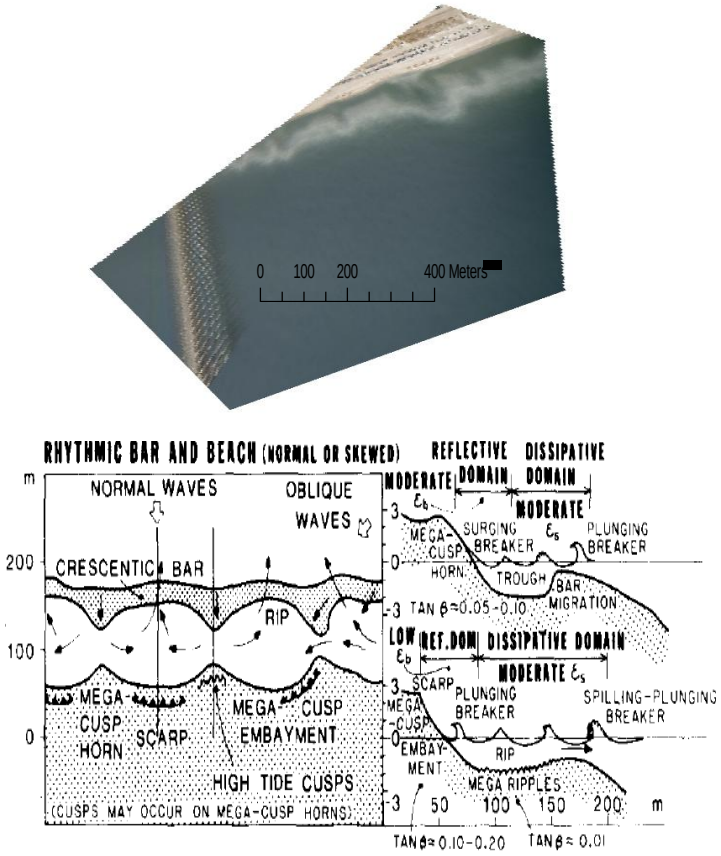

Figure 29: (Top) Image is from April 7, 2010, showing RBB morphology. (Bottom) Image was from Wright and Short (1984) depicting a RBB morphology.

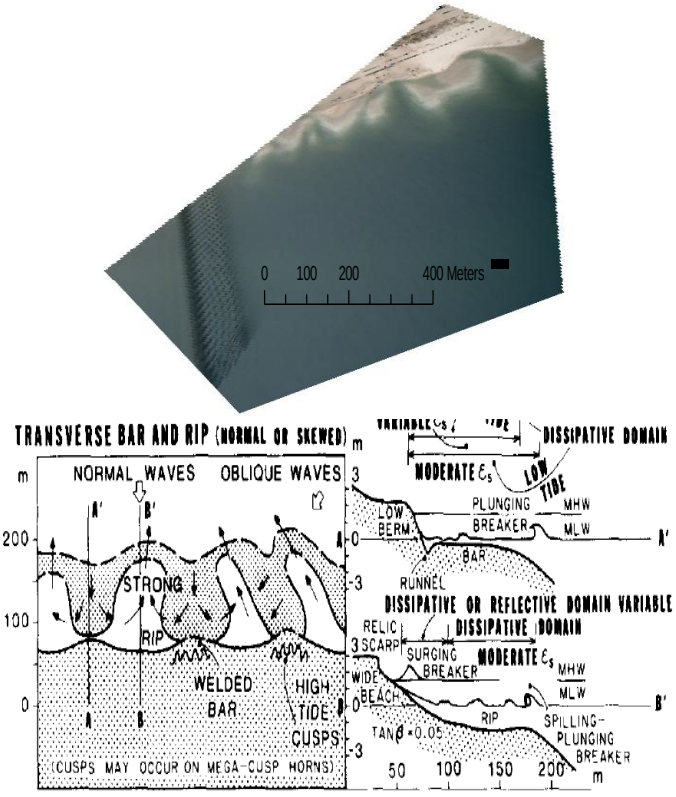

Figure 30: (Top) Image is from April 27, 2010, showing TBR morphology. (Bottom) Image was from Wright and Short (1984) depicting TBR morphology.

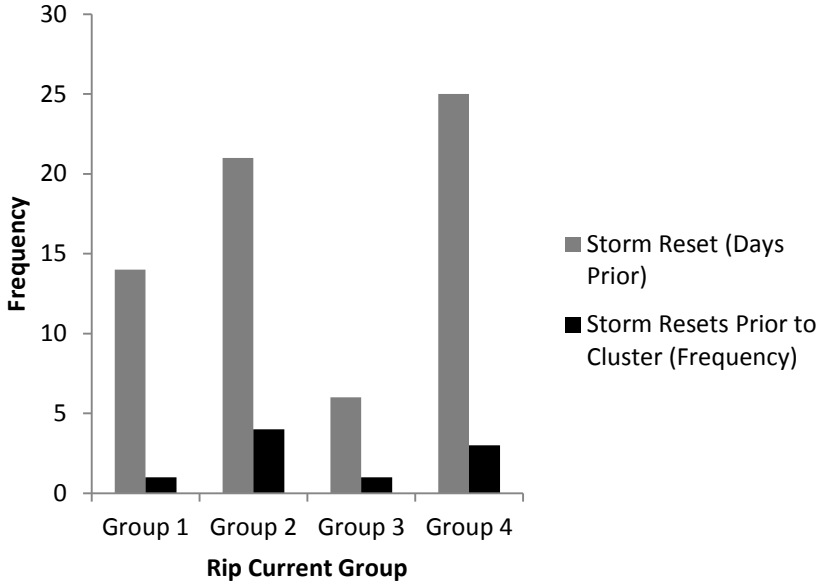

Figure 31: Bar graph showing the number of days which occurred between a reset storm and a cluster of rips and the number of reset storms which occurred before the rip cluster.

5.b Rip Characteristics

5.b.1 Rip Width

The table of rip widths for each rip channel can be seen below (Table 3) along with the table showing the mean rip channel width for each day (Table 3). Table 3 shows that the rip channel width varies from day to day and especially from rip current to rip current. The reason for this is related to the changing morphology of the rip channels from day to day and the alongshore variation in rip channel width across the surfzone. The rip channels infilled (decreasing in width) and eroded (increasing in width). The overall average of rip channel widths across the entire period of the study was 53 m. The largest mean rip channel width for a day was on morning of May 10, 2010 and was 105 m, while the smallest mean rip channel width was on May 4, 2010 with a mean of 27 m. The month with the largest mean rip width when there were multiple rip days was May (56 m), while the smallest mean rip width was in October (32.4 m). January had approximately a mean rip width of 50 m and April a mean rip width of 50 m. Finally, the July mean rip width was 64 m, which only was for one day of rip activity. The rip channels with the smallest widths would be associated with the greatest velocities, assuming all the rip channels had the same depth. For this study, October would have had the greatest mean rip velocities, while May would have had the slowest mean rip current velocities.

Table 3: Rip channel width in meters. The M beside the date signifies the morning stacked image and the A signifies the afternoon time of the same day. Far right column is the mean rip channel width for each time stacked image. Rips A through H are located in a west to east direction.

	Frequency	Width A (m)	Width B (m)	Width C (m)	Width D (m)	Width E (m)	Width F (m)	Width G (m)	Width H (m)	Mean Width (m)	Standard Deviation
10/31/2009	8	30	24	35	17	38	49	23	43	32	13
1/15/2010	3	75	70	83						76	37
1/22/2010	3	32	41	74						49	29
1/25/2010	3	35	33	72						47	28
1/29/2010	3	43	31	61						45	24
4/5/2010-M	6	31	21	38	24	111	39			44	34
4/5/2010-A	5	26	27	45	97	31				45.	31
4/7/2010	2	29	110							70	56
4/11/2010	7	25	33	39	90	48	36	52		46	24
4/13/2010	6	28	38	44	79	27	43			43	22
4/14/2010-M	5	45	77	37	31	46				47	23
4/14/2010-A	3	38	42	77						52	30
4/16/2010-M	1	60								60	42
4/16/2010-A	1	65								65	45
4/27/2010	6	22	22	23	27	76	70			40	27
4/30/2010	1	42								42	29
5/4/2010	2	20	33							27	16
5/5/2010-M	2	23	41							32	20
5/5/2010-A	2	25	41							33	20
5/10/2010-M	2	112	97							105	60
5/10/2010-A	2	106	8							94	54
5/11/2010	2	97	75							86	50
5/12/2010	2	73	55							64	37
5/14/2010	2	34	31							33	18
5/15/2010	2	36	45							40	23
5/17/2010-M	2	61	54							57	32
5/17/2010-A	2	50	49							49	27
7/13/2010	5	30	46	71	52	122				64	40

For the overall duration of the study there was an inverse relationship between the mean width of the rip channels on a given day and the frequency of rips on that day. This relationship can be seen in Figure 32. This relationship had a Pearson's product moment correlation coefficient (r) for the year was -0.298. Given that -1 would represent a perfect inverse relationship between the two variables the -0.298 would represent only a slight inverse relationship between the variables. The associated *p-value* with this relationship was 0.124. This means the relationship is not statistically significant. However, for the month of April, which consisted of the most rip channels, the Pearson's product moment correlation coefficient (r) was -0.666 (Figure 33). This value would represent a more significant inverse relationship. The *p-value* for the April mean widths versus the frequency was 0.025 showing a statistically significant relationship. Removing the month of May from the equation, the r value for the rest of the year's rips was 0.558, still showing a fairly significant inverse relationship between the mean rip width and rip frequency. The month of May consisted of a rip frequency that was constant throughout the month resulting in all of the points creating a vertical line. It is important to note that the method of width measurement may have a slight impact on the relationship seen. If a more accurate method (such as an automated edge detector) was used the rip widths may have changed. However, the difference in methods would not have resulted in a change in the overall relationship just the magnitude of it. Another influence on the relationship may have been the rectification itself. A more accurate rectification may have changed the relationship; however, the relationship seen is what is expected of a ridge and swale topography offshore.

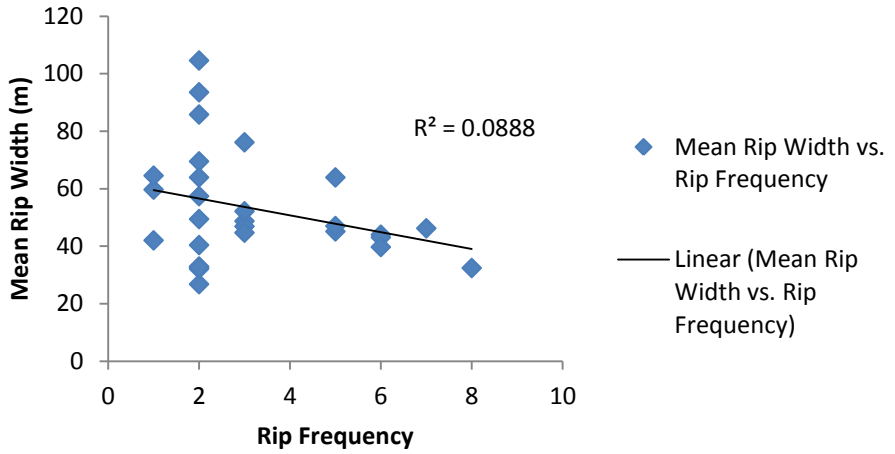

Figure 32: Graph showing the mean width of the rips on each day versus the frequency of rips on that day.

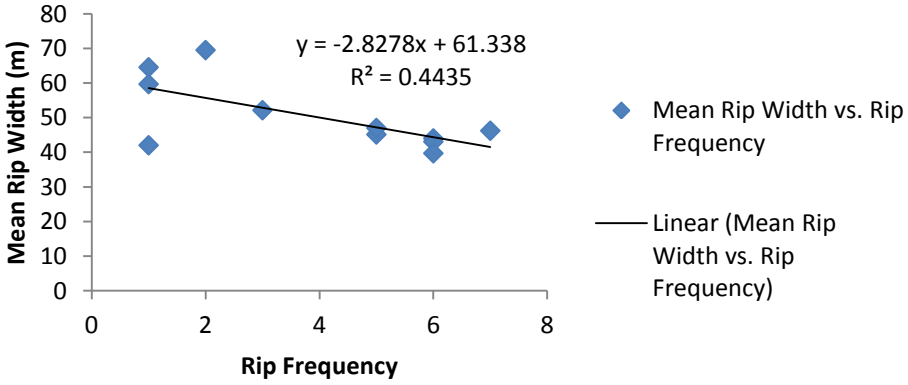

Figure 33: Graph showing the mean width of the rips on the days in April versus the frequency of rips on that day

5.b.2 Rip Current Angle

Table 4 shows the rip current angles over the course of the study. All of the rip channels had angles that were between the range of 120° and 214°, with the mean angle being 147° and in a southeast to northwest tending direction. The mean angle for each rip channel day can also be seen in Table 4. The outlier rip angle was on April 27, 2010. This day had a total of 6 rip channels with one being 214°, while the other rips were around the 140° angle. The 214° angle was associated with a rip channel that was part of a double rip channel. One rip was at an angle of 143°, while the outlier was oriented in a southwest direction (214°) instead.

The rip channel angle was fairly consistent from day to day, which is what would be expected. This is because once a rip channel formed it remained in place (semi-permanent) until it was infilled. The biggest differences between the mean rip current angles occurred following a reset storm. This is because the rip channels had been reconfigured and re-established at a different location and angle.

5.b.3 Rip Characteristics and Reset Storms

The impact of reset storms were analyzed for the width of the rip channels. Before the reset storm on January 16 there were 3 rip channels with a mean width of 76 m. Following the reset storm there were 3 days with rip channel (3 rip channels each

day), with the mean width decreasing to 47 m for the 3 days combined. Another change occurred in the rip width during a long period of recovery. Following the reset storm on March 11, the rip channels that appeared on April 5 started to reduce in frequency and width over the next month. The frequency started out around 5-7 rip channels and decreased down to 2 rip channels on May 4, which remained constant throughout the entire month. The rip widths associated with these rips started out at ~45 m and increased sporadically until it reach a max at 105 m in May.

The locations of the rip channels were examined to determine how far offshore the rip channels were developing before and after a reset storm. Before the reset storms on November 10, December 2, December 18, and December 24 in 2009, the average distance offshore that the rip channels developed was 43 m. After the 4 reset storms the rip channels on January 15, 2010 developed at an average of 45 m offshore. Then the next set of rip channels (January 22, 25, and 29) developed at an average of 46.56 m offshore following the reset storm on January 16, 2010. Finally, following reset storms on February 5, March 2, and March 11 of 2010, the next set of rips occurred at an average of 26 m offshore. It is important to note that the rips which developed after the reset storm on March 11 occurred 25 days following the storm reset giving plenty of

Table 4: Rip channel angles. Far right column is the mean rip channel angle for each day.

	Angle A	Angle B	Angle C	Angle D	Angle E	Angle F	Angle G	Angle H	Mean Angle	Standard Deviation
10/31/2009	199	126	192	114	205	119	108	139	150	41
1/15/2010	180	161	135						159	23
1/22/2010	210	136	124						157	47
1/25/2010	192	158	185						178	18
1/29/2010	180	158	147						162	17
4/5/2010-M	185	145	142	131	131	130			144	21
4/5/2010-A	214	145	142	131	131	130			149	33
4/7/2010	138	138							138	0
4/11/2010	186	189	154	136	138	132	130		152	25
4/13/2010	186	189	159	136	138	126	130		152	26
4/14/2010-M	161	135	134	129	127				137	14
4/14/2010-A	176	138	127						147	26
4/16/2010-M	161								161	
4/16/2010-A	171								171	
4/27/2010	124	197	143	214	141	138			160	37
4/30/2010	141								141	
5/4/2010	145	132							139	9
5/5/2010-M	135	131							133	3
5/5/2010-A	135	131							133	3
5/10/2010-M	135	131							133	3
5/10/2010-A	135	131							133	3
5/11/2010	135	133							134	1
5/12/2010	140	148							144	6
5/14/2010	138	131							135	5
5/15/2010	141	137							139	3
5/17/2010-M	150	133							142	12
5/17/2010-A	167	133							150	24
7/13/2010	141	141	133	120	124				132	10

time for bar migration back onshore. In general, rip channels developed between 1 and 2 m further offshore from the previous rip distances following a reset storm.

5.c Rip Channel Locations and Clustering

The map of rip channel locations (Figure 34) shows that the rip currents occurred throughout study area. These locations are the center of the visible rip channels over the course of the study. This map also depicts that there have been some hot spots or clustering of rip channel activity. The larger breaks between the locations of the rip channels could be the separation of the rip clusters. All rip channels between the reset storm on October 23, 2009 and the next reset storm on November 10, 2009 were classified as cluster 1. All of the rips in cluster 1 occurred on October 31, 2009. The second cluster occurred between storm resets on December 24, 2009 and January 16, 2010. The rips in cluster 2 occurred on January 15, 2010. Cluster 3 was bounded by the storm reset on January 16, 2010 and February 5, 2010. This cluster had rip currents occur on 3 different days, January 22, 25, 29. The last cluster of rips occurred following a storm reset on March 11, 2010, but was not bounded by another storm reset because the year study concluded before the next reset. These rips occurred on April 5, 7, 11, 13, 14, 27, and 30; May 4, 5, 10, 11, 12, 14, 15, and 17; and July 13. A map showing the clustered rip currents by reset storms can be seen in Figure 35. From the map showing rip clustering based on reset storms, it can be determined that the rip channels developed

Figure 34: Map showing the locations of all the rip channels observed during the study.

Each green dot represents a rip channel.

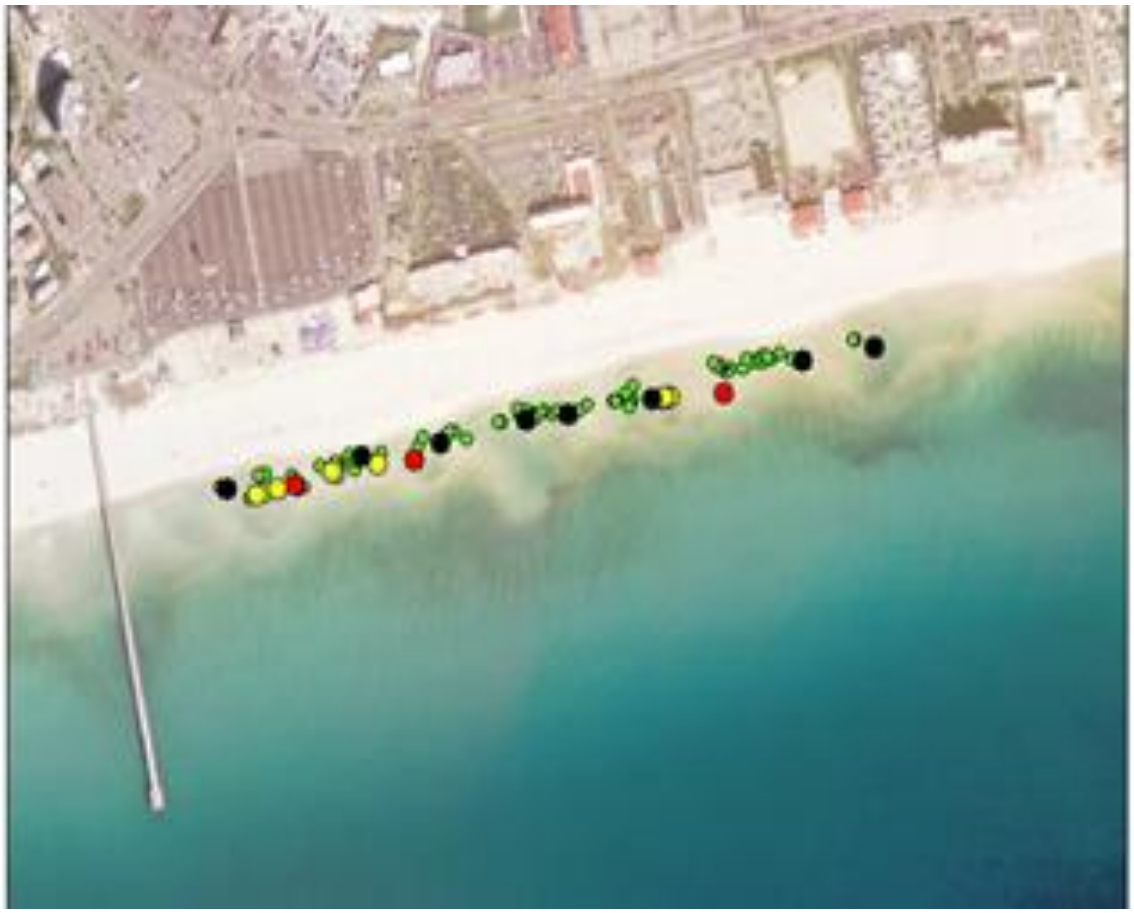

Figure 35: Map showing rip clusters based on reset storms (temporal). Black circles represent cluster 1, red circles cluster 2, yellow circles cluster 3, and cluster 4 being green circles.

at approximately the same locations from one reset to the next. From this map it can also be seen that the majority of rip currents occurred during one cluster. This is the cluster that includes all of the rip currents that occurred during April and May.

To determine clustering spatially, an agglomerative hierarchal cluster analysis was used. The UTM coordinates for each rip were entered into the hierarchal cluster analysis to determine if there was clustering of the rips across the nearshore. The clusters resulting can be seen in Figure 36 and the mean location of each cluster in Figure 37. This cluster analysis shows spatial clustering alongshore, where Figure 35 above showed the clustering on a temporal scale. The spatial cluster analysis showed there were a total of 7 rip locations, with an average spacing of 113 m. Starting from the west the clusters were number 1 to 7, of which the rip channel mean angles and rip width can be seen in Table 5. Cluster 1 contained 12 rip channels with a mean angle of 180° and mean rip width of 34 m, while the cluster spanned 60 m. Cluster two was associated with 11 rip channels, a mean angle of 158°, and a mean width of 33 m. Cluster two spanned a total distance of 65 m. Cluster 3 was associated with 10 rip channels with the mean angle being 152°, a mean rip width of 40 m, and a range of 62 m. Cluster 4 contained 19 rip channels with a mean angle of 149°, a mean rip width of 54, and spanned a distance of 101 m. Cluster 4 had the largest range meaning the locations of the rips spanned the largest section of the nearshore compared to the other clusters. Cluster 5 contained 12 rip channels at a mean angle of 136°, a mean rip width of 79 m, and a range of 44 m. Cluster 6 contained the most rip channels at 22 at a mean angle of 132°, a mean rip width of 56 m, and a range of 97 m. The last cluster, Cluster 7 contained the fewest rip channels at 4 containing a mean angle of 131°, a mean rip width of 46 m, and a range of 19 m. Cluster 7 spanned the smallest length of the nearshore.

Figure 36: Map showing rip channel spatial clustering. Each color represents a separate cluster.

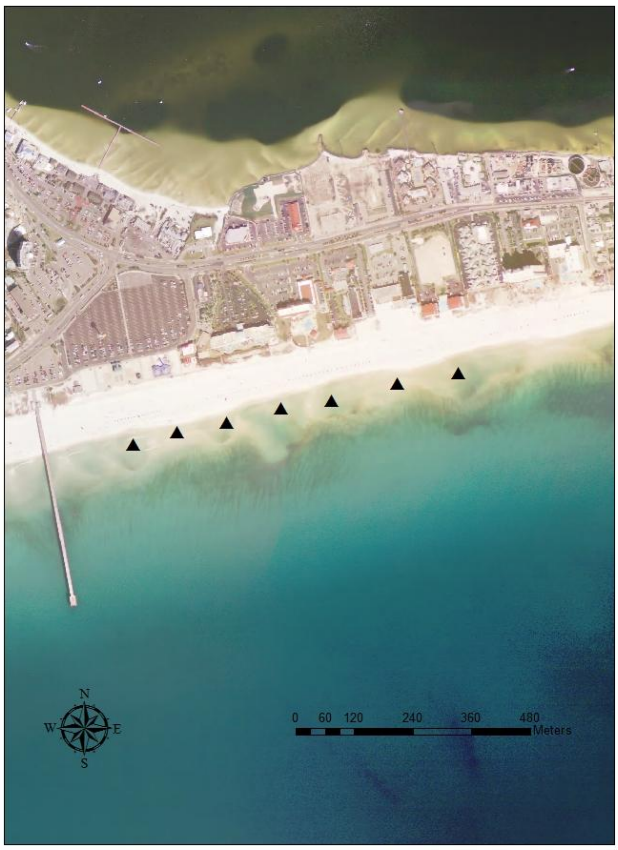

Figure 37: Map showing the mean centers of the above rip channel clusters.

There is a high probability that if there was a rip current that it would fall near one of the 7 clusters. The spatial autocorrelation test Moran's I was used to determine if the clustering in Figure 36 was significant. The Moran's I value came to 0.68, which would describe a clustered pattern, given that Moran's I values near 1 and -1 both represent perfect clustering and a value of 0 represent complete dispersion of the points. The spatial autocorrelation also determined that this value was statistically significant on a 95

percent confidence level based on a z-score of 8.78 and a p-value of 0. The high z-score (above 1.96) and low p-value (below 0.05) describes a scenario where there is a greater than 95 percent chance that the null hypothesis, "there is no spatial clustering and the points are completely randomized," is rejected.

Table 5: The mean rip angles, widths, associated standard deviations and range for each cluster.

	Mean Rip Angle (°)	Standard Deviation in Mean Angle	Mean Rip Width (m)	Standard Deviation in Mean Width	Range (m)
Cluster 1	180	25	34	14	60
Cluster 2	158	26	33	7	65
Cluster 3	152	18	40	13	62
Cluster 4	149	25	54	29	101
Cluster 5	136	17	79	20	44
Cluster 6	132	7	56	29	97
Cluster 7	132	6	46	4	19

5.d Wind and Wave Characteristics

Buoy data (Table 6) showed that the mean wave height associated with rip channel development in the study area was 0.90 m. The maximum wave height associated with the rip channel development was 1.58 m, while the minimum wave height was 0.48 m. The range of wave heights was between 0.48 m – 1.58 m. The overall mean wave height was calculated by averaging the wave heights for each day in which rip currents appeared. The wave direction associated with the rip channel days (Table 6) shows that on the majority of days which rip channels appeared, the mean wave direction was from the southeast direction, which was the same as the most

common rip channel angle mentioned previously. 18 of the 28 times in which rip currents developed, resulted in the wave angle and rip current angle being within 30 degrees of each other.

The wind data (Table 6) shows that when the wind was from the southern direction there were higher instances in which rip currents developed. 20 of the 28 rip current occurrences showed wind coming from the south. This ranged from the east-south-east across to the west-south-west. The wind speeds (Table 6) during rip channel development had a wide range of values, counter to the values seen for wave height, wave angle, and wind direction. The average wind speed was 2.99 m/s, but the range of wind speeds was from 0.45-5.81 m/s.

The surf similarity parameter (Ω) shown in Table 6 describes the beach state on each time of day that had observable rip channel activity. Of the 28 occurrences 22 were expected to be in an intermediate beach ($1 < \Omega < 6$). The other occurrences were expected to be in a reflective state ($\Omega < 1$). However, at least 4 of the days that were classified as reflective were most likely in transition between the intermediate beach state and the reflective beach state due to the surf similarity parameter being near 1. All of the observed beach states were intermediate. Each rip channel day had a clearly developed bar and rip channels, all of which would fall under the intermediate beach states, longshore bar and trough, rhythmic bar and beach, or transverse bar and rip.

Table 6: Wave heights associated with days which developed rip channels along with the mean wave angle, wind speed, and direction. The surf similarity parameter associated with each day is based off of the equation $\Omega=H/(w_sT)$, where H is the offshore wave height, ws is the sediment fall velocity and T is the wave period. The far right column is the expected beach state based on surf similarity parameter

	Wave Height (m)	Mean Wave Angle (°)	Wind Speed (m/s)	Wind Direction	Surf Similarity Parameter	Expected Beach State	Observed Beach State
10/31/2009	1.20	124	5.36	NNW	1.79	Intermediate	Intermediate
1/15/2010	0.75	139	3.58	NE	1.27	Intermediate	Intermediate
1/22/2010	1.20	143	1.79	WNW	2.07	Intermediate	Intermediate
1/25/2010	1.58	103	3.58	W	2.75	Intermediate	Intermediate
1/29/2010	0.89	47	4.92	SE	1.55	Intermediate	Intermediate
4/5/2010-M	0.48	323	1.34	SSE	0.86	Reflective	Intermediate
4/5/2010-A	0.48	323	1.34	SSE	0.86	Reflective	Intermediate
4/7/2010	0.81	324	5.81	SSE	1.46	Intermediate	Intermediate
4/11/2010	0.61	316	1.79	ESE	1.13	Intermediate	Intermediate
4/13/2010	0.71	316	2.68	ESE	1.33	Intermediate	Intermediate
4/14/2010-M	0.89	317	3.58	ESE	1.70	Intermediate	Intermediate
4/14/2010-A	0.89	317	3.58	ESE	1.70	Intermediate	Intermediate
4/16/2010-M	1.17	304	2.24	SSE	2.25	Intermediate	Intermediate
4/16/2010-A	1.17	304	2.24	SSE	2.25	Intermediate	Intermediate
4/27/2010	0.65	14	1.79	NW	1.22	Intermediate	Intermediate
4/30/2010	1.20	101	5.36	SE	2.22	Intermediate	Intermediate
5/4/2010	1.04	220	2.24	NE	1.92	Intermediate	Intermediate
5/5/2010-M	0.70	249	0.45	SSW	1.29	Intermediate	Intermediate
5/5/2010-A	0.70	249	0.45	SSW	1.29	Intermediate	Intermediate
5/10/2010-M	0.61	325	3.58	ESE	1.13	Intermediate	Intermediate
5/10/2010-A	0.61	325	3.58	ESE	1.13	Intermediate	Intermediate
5/11/2010	0.96	329	4.47	SSE	1.78	Intermediate	Intermediate
5/12/2010	1.06	10	4.92	SE	0.87	Reflective	Intermediate
5/14/2010	1.11	14	2.68	ESE	0.92	Reflective	Intermediate
5/15/2010	1.27	18	4.47	SE	1.05	Intermediate	Intermediate
5/17/2010-M	0.79	349	1.34	W	0.65	Reflective	Intermediate
5/17/2010-A	0.79	349	1.34	W	0.65	Reflective	Intermediate
7/13/2010	0.77	147	3.13	WSW	1.32	Intermediate	Intermediate

In Figure 38 below, the graph shows that there is an inverse relationship between rip current frequency on a given day and the surf similarity parameter. As the surf similarity parameter increases, the rip frequency for that day decreases and vice versa. The Pearson's product moment correlation coefficient (r) was -0.167 for the entire data set with a *p-value* of 0.394. For the month of April there was a Pearson's product moment correlation coefficient (r) of -0.848. The r value for the entire data set shows a slight inverse relationship between the rip frequency and surf similarity parameter. The r value for the month of April again shows a significant inverse relationship between the two variables and based on the *p-value* of 0.000098 is statistically significant. The inverse relationship was not evident in May due to all of the days only having 2 rip currents. As noted previously, the beach state with the lowest frequency of rips is expected to be that of a longshore bar and trough which has a higher surf similarity parameter. While the larger frequency of rips is expected to be in a transverse bar and rip beach state, which usually has a smaller surf similarity parameter. For this study, the two largest frequencies of rip channels were on October 31, 2009 (8) and April 11, 2010 (7). October 31 had a surf similarity parameter of 1.79 and April 11 had a surf similarity parameter of 1.13, both days of which were in a transverse bar and rip state. Other days, for example January 25, 2010 (3 rips) and April 16 (1 rip) had larger surf similarity parameters. Specifically, January 25 had a surf similarity parameter of 2.75 and April 16 had one of 2.25. Both of these days were in a longshore bar and trough beach state.

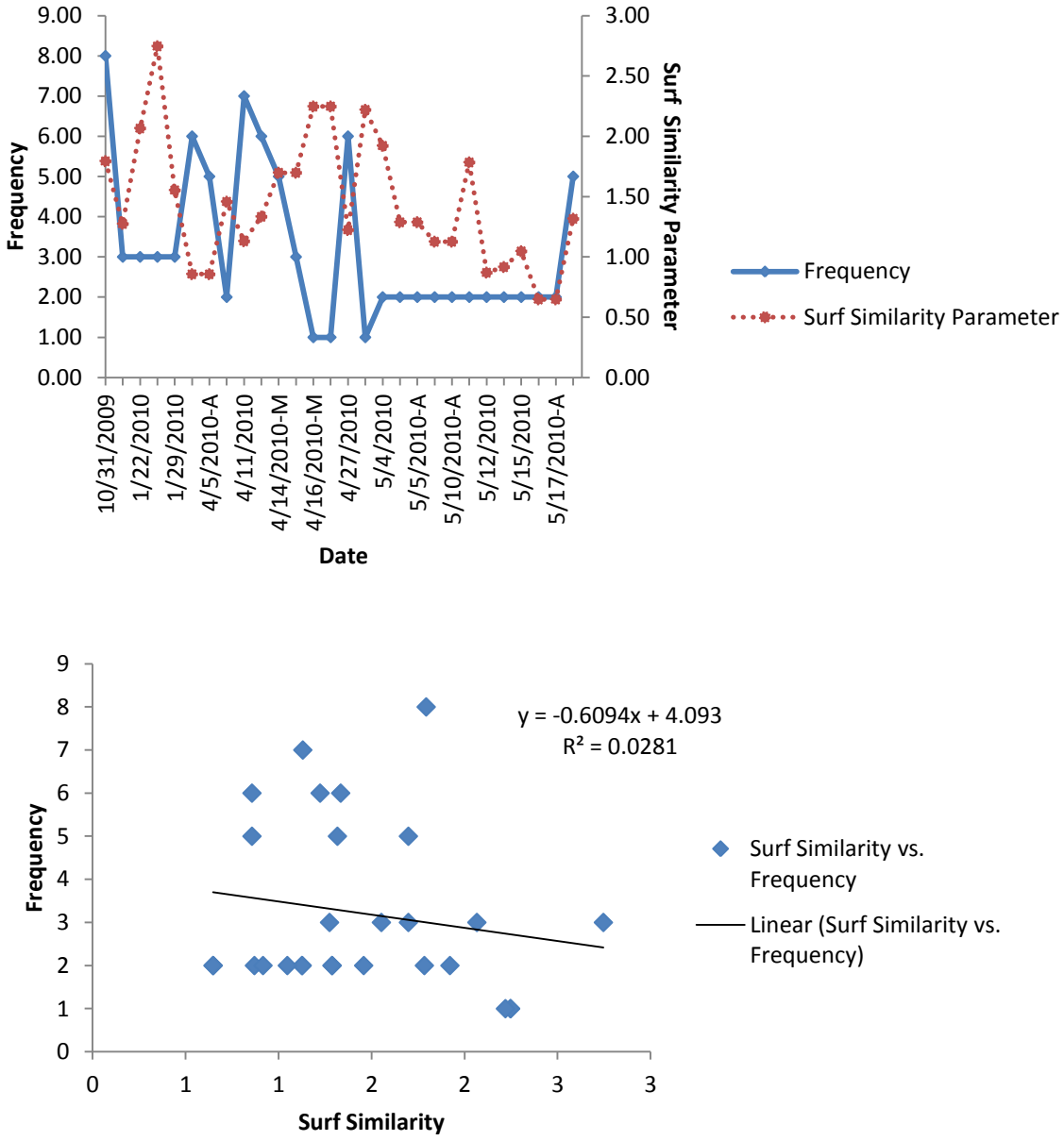

Figure 38: (Top) Graph showing mean surf similarity parameter for each day which rip channels occurred (Dashed Line) along with the amount of observed rips for each of those days (Solid Line). (Bottom) Scatterplot showing surf similarity versus rip frequency

The surf similarity parameter was also compared to the mean rip width for each rip channel day (Figure 39). Unlike the frequency and surf similarity parameter there was no apparent relationship and the Pearson's product moment correlation coefficient was -0.07, which means there was no significant relationship between the two variables. This relationship proved not to be statistically significant with a *p-value* of 0.731.

Figure 40 depicts a comparision of the mean rip angle and the surf similarity parameter. There was a moderate positive relatsionship between the two variables, with a Pearson's product moment correlations coefficient of 0.48. The relationship between the mean rip angle and surf similarity parameter was statistically significant based on the calclulated *p-value* of 0.009. Meaning that as mean rip angle increased so did the associated surf similarity parameter. This relationship was statistically significant based on the *p-value* above.

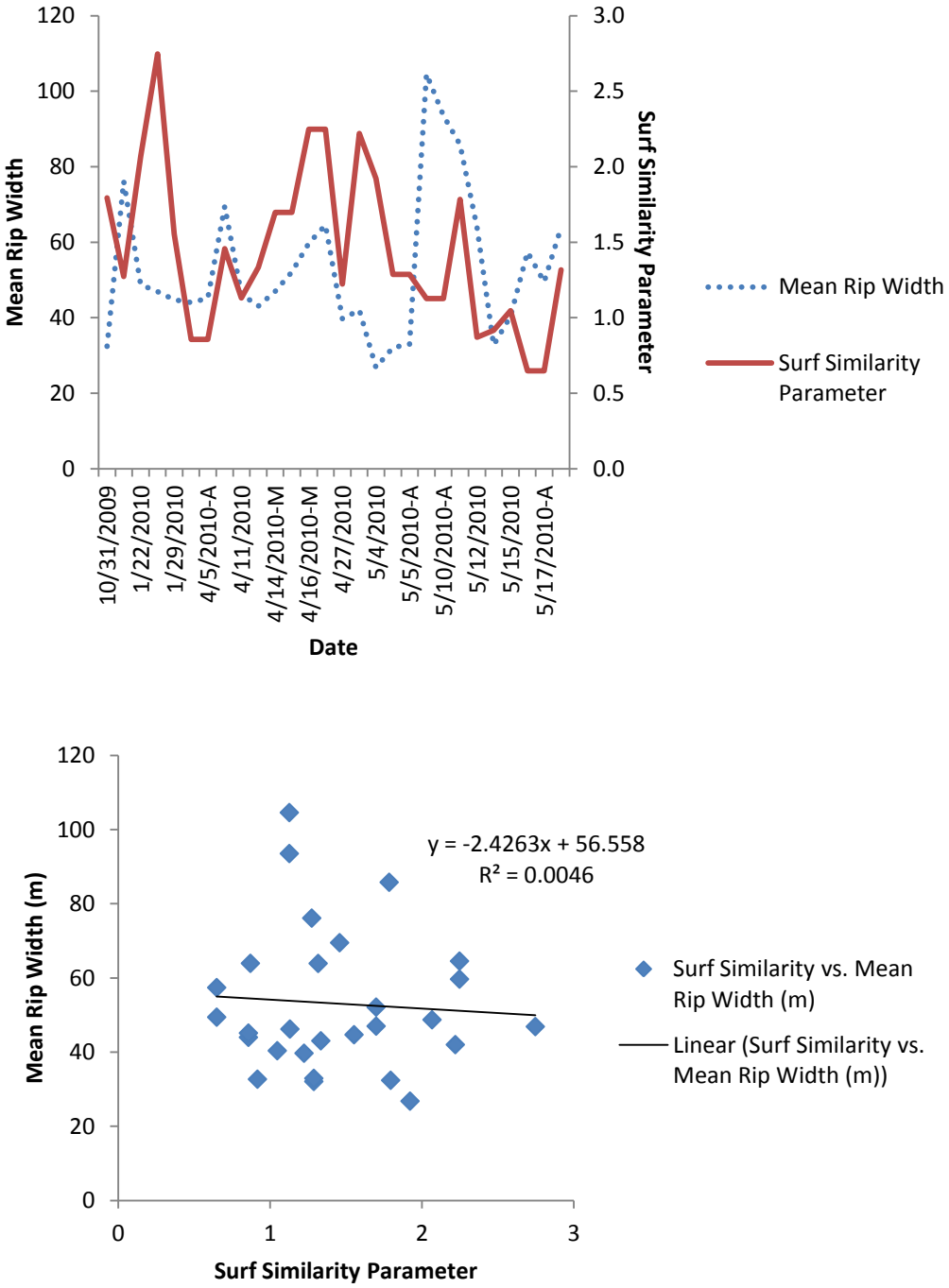

Figure 39: Line graph comparing mean rip width versus the surf similarity parameter.

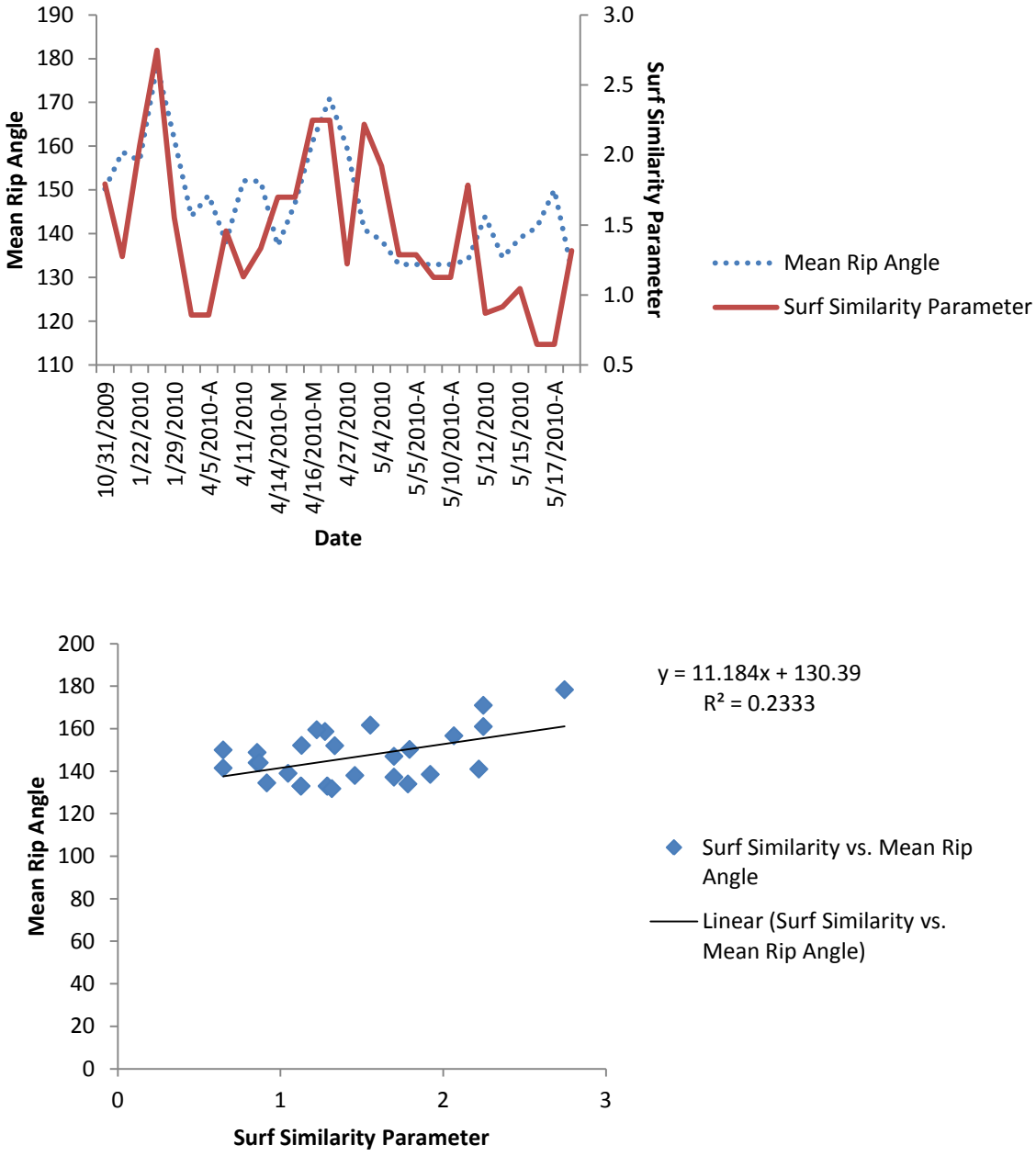

Figure 40: Line graph comparing mean rip angle versus the surf similarity parameter.

CHAPTER VI

DISCUSSION

This study has shown that over a course of a year the nearshore system at Pensacola Beach, and specifically Casino Beach, transitions through multiple beach states with varying rip frequencies. The cycling of beach states is a direct result of frontal storms and tropical systems through the year. Beginning in early October and then in November with the landfall of Tropical Storm Ida, Casino Beach went through 9 reset storms all of which had a similar impacts on the bar and rip morphology. Following each reset storm the inner bar would start to move back onshore or reconfigure and cycle through the intermediate beach states described in the Wright and Short (1984) model. As their model described, the probability of rip currents increase as the beach state moves from longshore bar and trough to the transverse bar and rip state, which has the highest probability to produce strong rip currents. Although the exact velocity was not measured for this study, it can be inferred that the transverse bar and rip states observed at Casino Beach resulted in the strongest velocities in the rip channels (Brander and Short, 2000). This is due to this beach state having the smallest width of rip channel. Assuming all the rip channels had the same depth a rip current would be stronger with a smaller width of the rip channel. Immediately following a reset storm, the beach state was most frequently a rhythmic bar and beach then as the bar migrated onshore it changed to the transverse bar and rip state. Rip channels and rips started to develop with a rhythmic bar and beach state. It took on average 24 days of bar

migration and no storm activity for the beach state to turn into a transverse bar and rip state following a rhythmic bar and beach state based on the shape of the bar. The largest time for the beach state change was 46 days, while the shortest was 5 days. The difference was most likely a result of the wave conditions between the beach state changes. The largest time between beach state changes occurred during the winter, where multiple reset storms transpired. The winter reset storms continued moving the sand bar offshore for a month and a half but the beach state remained in a longshore bar and trough state. The short time between beach states occurred following a reset storm. The storm caused the beach to change into a rhythmic bar and beach state. However, the reset storm did not pull the bar far offshore so it only took 5 days to reform back into a transverse bar and rip state.

The transverse bar and rip state is the one that dominated Casino Beach and had the most observable rips, which correlates exactly to the Wright and Short (1984) beach state model. The only observable occurrence of a longshore bar and trough state changing to a rhythmic bar and beach was due to a storm causing the bar to migrate onshore. The other occurrences between reset storms did not see an observable change in beach state. The average time between the reset storms was 17, most likely not allowing enough time for enough bar migration to change beach states. This research has further reinforced the Wright and Short (1984) model confirming that large frontal storms and tropical storms can reset the nearshore morphology and beach state, which over time will recover and continue to cycle back through the beach states. In this

respect the reset storms had a direct impact on when the rip hazard at Pensacola Beach was the greatest.

This research has also found that the majority of rips (77 percent of all rips) occurring along Casino Beach were during the spring and summer months. This leads to an increase in the risk posed to beach goers during these months, which is the primary tourist months on Santa Rosa Island. With the increase in beach goers and the dramatic increase in rip currents during the spring and summer, there is an increase in the risk for drowning at Casino Beach. However, there is the lack of consistent rip development in the summer months. This is most likely a result of there being zero reset storms which occurred during the summer. Normally, tropical cyclones are the type of reset storm that could occur in the summer months to cause a reset, but during this study zero tropical cyclones made landfall during the summer of 2010. The inner bar almost completely attached to the beach causing less favorable nearshore morphology for rip development due to the decrease in distinct rip channels. As a result, during the study spring was the worst time for rip current activity. The evidence showing 7 accretional rip channel clusters is consistent with the study conducted by Houser, Barrett, and Labude (2011a). Their study showed that offshore transverse ridges focused wave energy and caused a clustering of rip development between ridges. Casino Beach is one of these hotspots in which there was a statistically significant cluster of drownings associated with rip currents. This research has shown that there is a clustering of locations of rip channel development inside of the Casino Beach hotspot. The 7 cluster locations were shown to be significant at the 95 percent confidence level with spacing at approximately 113 m

apart. If a rip channel were to develop, there is a high likelihood that it would be located near one of the 7 clusters indicated previously. The statistical behavior of these 7 rip clusters varied across the nearshore. The average widths of the rip channel clusters from west to east were 34 m, 33 m, 40 m, 54 m, 79 m, 56 m, and 46 m. These were the average widths of the rip channels located within a cluster. Spatially, the highest frequency of rips occurred in the cluster with an average width of 56 m and the lowest frequency occurred in the cluster with the average width of 46 m. Aside from the farthest east cluster, generally the rip frequency of each cluster was higher on the eastern side of the study site.

The most interesting aspect of the rip clusters is the locations are consistent throughout the year, despite multiple reset storms reworking the sand bar. This means that the rip channels are occurring at similar locations in October as they are in April. One possible reason is due to the wave forcing caused by the offshore ridge and swale topography at Casino Beach (Houser, Barrett, and Labude, 2011). The ridge and swale topography along with wave forcing has resulted in the bar attaching to the shoreline at roughly the same locations throughout the year. When this occurs the resulting rip channels will have fairly consistent locations throughout the year causing clusters of rip channels to appear over time. Also, given that through the majority of the year, Pensacola Beach receives similar weather and wave conditions the migration of the bar in the nearshore should be somewhat consistent between different months. Essentially, due to the ridge and swale topography creating a lower energy environment in the swales, the bar migrates onshore in a similar pattern throughout the year. The lowest

wave heights are seen in the middle of the swales, which one of these points is Casino Beach. When the bar eventually attaches to the beach face it occurs at approximately the middle of the swale and the rest of the points of bar attachment (during a TBR state) organizes itself off of the first attachment. Since this pattern of attachment is repeated and the smallest waves occur at the same locations the rip channels will develop at similar locations throughout the year with the location of the first attachment being the most preferred location. This location was the spot of the most dominate rip which would develop.

The existence of preferred or consistent rip locations is one that has been explored in past studies such as Holman *et al.* (2006) and Short (1985). The Holman *et al.* (2006) study found no evidence to suggest preferred rip locations over a course of 3 years and ~6,000 rips. However, Short (1985) found that persistent rip locations can vary depending on the beach state. They found two beach states exhibit persistent rip locations over time, RBB and TBR. On the other end of the spectrum they found that LBT and D beach states exhibited no evidence for preferred rip locations. The current study was unique because it showed that at Pensacola Beach there are preferred locations for rip development, which was consistent throughout all beach states. These locations occurred over one year and were not impacted by a very large reset storm (hurricane), which would have resulted in limited rip activity follow an extremely large reset storm.

The mean rip width associated with the rip channels decreased in width based on the observed beach state. For example on January 15, 2009, which was a longshore bar and trough beach state, the mean rip width was ~76 m. As described in the Wright and

Short (1984) model and confirmed by Short (1985) and Brander (1999), the mean rip width for a transverse bar and rip state is expected to be smaller, which October 31, 2009 was at ~32 m. All three studies mentioned above showed that as the bar migrates onshore during beach recovery the observed rip channel widths decreased. Therefore, longshore bar and trough states are expected to have the largest rip widths and the smallest rip widths are observed in the low tide terrace beach state. This same relationship was seen throughout this study and data, where the rhythmic bar and beach states had rip channels larger than the transverse bar and rip and smaller than the longshore bar and trough. This also leads to the assumption that the transverse bar and rip state has the strongest rips. Given that there is equal depth, the smaller rip channel widths of the transverse bar and rip beach state will have the largest rip velocities.

Results of the study also suggest that in a given area of rip channel development there is variability in the rip channel development on a temporal scale. At Casino Beach, the rip current development is almost nonexistent in the fall and winter months. Only 4 days out of the total of 181 days during the fall resulted in a visible rip channel. This can be explained by the large amount of frontal storms that resulted in resets of the beach state regularly. Rip channel development was most frequent in April and May due to there being a lack of a reset storm. Without a reset storm, the beach states were able to cycle from a longshore bar and rip morphology with a few rips to a transverse bar and rip morphology with an increased amount of rip development. Frontal storms were an important phenomenon in determining when and how frequent the rip channel activity was at Casino Beach. As noted earlier, a reset storm is a storm event that results in the

destruction and subsequent regeneration of the sand bars and rip channels. These storm events caused the destruction and regeneration of the sand bars and rip channels by causing alongshore sedimentation of the existing rip channels and the eroding and opening up of new ones. Due to the high frequency of reset storms in November and December (4) there were no rip channel activity until mid-January. Again due to 3 reset storms in February and March there was another long span of zero rip channel activity until April. As a result of no reset storms after March 11, 2010 there was a high frequency of rip channel activity in April, May. This study defined a reset storm as one that had a wave height of 2.35 m. This was determined by averaging the wave heights associated with each reset storm observed over the study.

The surf similarity parameter and the imagery collected were almost identical in terms of beach state. The expected beach state from the surf similarity parameter matched exactly with the observed images on the days which rips developed a total of 22 of the 28 instances used. However, the 6 times in which it did not correlate with the imagery, the surf similarity parameter was close enough to 1 that there is to be some expected delay before the intermediate beach state would become a reflective beach state. For example the surf similarity parameter on April 5, 2010 was 0.86, which should represent a reflective beach state. However, the observed beach state showed an intermediate beach state, specifically a transverse bar and rip morphology. This is consistent with Short (1985) who observed a similar occurrence where the observed beach state was intermediate, but the surf similar parameter was less than one and the expected beach state was to be reflective.

In looking at the relationships of rip width, frequency, and surf similarity parameter there were no statistically significant relationships between the rip width vs. frequency or between the surf similarity parameter and frequency. Based on Holman *et al.* (2006) one would expect to see statistically significant relationship between the two comparisons based on a uniform beach. However for the entire data sets this relationship was not seen. This was most likely was caused by the ridge and swale topography creating a non-uniform beach. Contrary to the entire data set, the month of April did see a statistically significant relationship between rip width and frequency, as well as between surf similarity parameter and rip frequency. This relationship occurred as a result of there being no reset storms after March 11. Without a reset storm the bar migrated onshore eventually attaching at spots creating a TBR state. Without a reset storm there was a more uniform state resulting in the relationships to become statistically significant. Like the Wright and Short (1984) model there was an increase in rip frequency and decrease in rip width as the bar migrated onshore uninterrupted. It is important to note that the Wright and Short (1984) study was done over a three year time period and the Holman *et al.* (2006) study spanned four years. Meaning both studies had larger data sets and saw uniform beaches. This study only had a data spanning one year, with a much smaller data set. However, due to the ridge and swale topography the relationships above would be expected on longer time scales such as 5 and 10 years.

The seasonal difference in rip frequency found throughout the study adds to the idea that the spring and summer months pose the greatest risk to beach goers. This is consistent with the Gensini and Ashley (2009), who showed that the rip hazard is

greatest in summer and spring months due to increased tourist activity along the beaches and the abundance of fair weather conditions. The major difference this study has shown was that the majority of rip channels occurred in April and May (spring). April and May had 64 observable rip channels, while June, July, and August only had 5. This would lead to the assumption that spring was a higher risk for drowning then was summer due to the largest amount of rips during this time, contrary to Gensini and Ashley (2009), which showed that summer, was the highest risk of all the seasons. The Gensini and Ashley (2009) study determined the largest risk to be on summer weekends mainly due to large amounts of tourists and social vulnerabilities were the highest. The main cause for the difference was that in this study there were zero reset storms which occurred after March 5, 2010. This caused the bar to migrate onshore leading to a transverse bar and rip state in April and May, because there were no more storm resets the bar was able to attach to the shoreline in June resulting in a reflective beach state and almost no rip channels for the rest of summer. If there had been more reset storms in March, April, or May there would have been a higher frequency of rip channels in the summer months.

The other difference in rip channel frequency occurred in May 2010. This month had a consistent rip frequency, which was a result of the beach state remaining the same throughout the entire month with no reset storms occurring to change the beach state. The lack of variation in the rip frequency caused all resulting statistics to be inaccurate because the r value cannot be calculated for a vertical line (constant frequency). For this reason the month of May was removed when calculating the r value for the mean rip

width and rip frequency relationship. May was different because there were no reset storms after the beginning of March allowing for almost full recovery of the beach. If the beach system had not fully recovered by the end of May, then June, July and August may have continued the trend of consistent rip frequency until the beach did recover or a reset storm occurred.

Looking at study sites and in particular how edge waves impact them, it can be seen that compared to studies in Australia (Wright and Short, 1984; Short 1985) and studies done off the coast of California (Bowen, 1967) where edge waves are extremely influential in cusp and rip formation, this research in the Gulf of Mexico had less of an impact by edge waves. This was seen in the lack of cusp formation throughout the year examined.

The use of the many old and new techniques were vital in creating rectified images that could be used in the analysis and examination of the rip current activity at Casino Beach. Techniques such as traditional surveying, GPS coordinate collection, ArcMap rectification, and time-stacking of the images have all been used in previous studies as methods to determine rip current locations, bar morphology, beach state, and rip current characteristics (rip width, spacing, and angle). One such study is Holman *et al*. (2006). Holman *et al*. (2006) used these techniques to look at the frequency, width, spacing, and duration of rip currents. Like Holman *et al*. (2006), the technique of time-stacking images was applied to an entire year's worth of images to analyze the variability of rip development over the course of an entire year. This technique was able to show visually how the beach state changed throughout and entire year from a

longshore bar and trough to a reflective beach state and everything in between. A new program was used to rectify coastal imagery that had previously been untested. The Georeferencing of Mountain Photography program was used to initially rectify the time-stacked images. This program had previously been used only for imagery taken in mountainous regions or imagery in areas of high elevation. The Georeferencing of Mountain Photography program had never been used on imagery taken at the coastline/coastal zone, which has an almost constant elevation with very little elevation change on the surface. This study had shown that the program can be very useful in producing fairly accurate rectified image of the coast.

This study has shown that the rip current development at Pensacola Beach, specifically Casino Beach, is dependent on many factors. These factors include, frontal storms, time since pervious frontal storm, wind angle, and beach state. These factors also had an influence on the rip frequency, width, spacing, and angle. Frontal storms impact the beach states, causing the bar to migrate offshore and begin the intermediate beach cycle over again. The time between frontal storms allowed for the development of rip channels and the change in beach states. As the bar migrates back onshore and eventually resulted in a transverse bar and rip state more and more rips began to develop. The wind angle was a factor, because rip currents primarily developed when the wind was coming from a southerly direction.

CHAPTER VII

CONCLUSION

The goal of this research was to examine the relationship between rip channel development and nearshore morphology along with the conditions under which the rip channels developed. To accomplish this, a combination of remote imagery and wind and wave forcings were examined. Highly oblique remote imagery had to be rectified to a planar view in order to examine the locations, widths, angles, and frequencies of rip currents over the period from September 24, 2009 to September 24, 2010. Buoy data was used to gain a better grasp as to what wave climates resulted in rip channel development and weather station data was used to better understand the wind forcings associated with the rip development as well. The first objective of the research was to quantify and characterize the behavior and development of accretion rips at Pensacola Beach over a year (9/24/09-9/24/10). The results of this research has shown that

1) At Casino Beach reset storms resulted in the reconfiguration of the sand bar and the rip channels. This reconfiguration subsequently resulted in a change in beach state. All of the observed reset storms occurred between October 2009 and March 2010. There were zero observed reset storms between April 2010 and September 2010. The absence of reset storms between April and September allowed for the sand bar to migrate onshore leading to further bar migration and

beach state cycle changes. The continued beach state changes toward the transverse bar and rip state lead to an increase in rip channel development.

2) The transverse bar and rip state had the smallest widths for the rip channels, while the largest widths occurred during longshore bar and trough beach states. Assuming that all rips had the same depth, that would mean that the transverse bar and rip beach state rips would have been the strongest.
3) The surf similarity parameter and imagery showed that Casino Beach was in an intermediate beach state for almost an entire year. The surf similarity parameter was also shown to not be related to rip frequency on the days in which rip currents were visible. However for the month of April there was a statistically significant relationship. The smaller the surf similarity parameter the larger the rip frequency. These relationships are not expected to change over longer time periods as long as there is a ridge and swale topography and reset storms.
4) April and May resulted in the largest rip frequencies as a result of zero frontal storms occurring after the beginning of March 2010 to the end of the study. The summer months of June, July, and August only had one day of rip channel activity because there were no reset storms to pull the bar offshore and start the intermediate beach state cycle again. The bar was almost completely attached during the summer months resulting in a more of a reflective beach state and no rip channel development. The location of the rips continued to move closer to the shoreline throughout the months of April and May. These results were a model of the period examined. From year to year the timing of reset storms

could be such that the most frequent rip channels appear in the summer months rather than the spring.

5) Large and frequent reset storms which occurred in the fall and winter months caused the sand bar to constantly move offshore not allowing for consistent bar migration and rip development. This resulted in very few observed rips between September 2009 and March 2010. However, the migrations of the bar and subsequent rip development during this time as well as over the course of a given year may vary year to year based on the timing, frequency, and severity of reset storms.

The second objective was to determine the variation in rip hazard over a year (September 2009 – September 2010). Specifically, the frequency, location, width, angle, and conditions under which the rips develop. The results of the research has shown

1) Rips developed in all four seasons (fall, winter, spring, and summer). However the majority of rips occurred in the spring (64) compared to fall (8), winter (12), and summer (5). The frequency of rips on a given day was not inversely related to the mean width of the rips on that day. This was correlated with a Pearson's product moment correlation coefficient (r) of -0.3. However, for the month of April this relationship had an r value of -0.7 and was statistically significant. This meant, the more rips that were observed, generally the smaller the mean width of the rips were for that day. The overall relationship between rip

frequency and rip width is not expected to change over longer periods as long as the ridge and swale topography remains offshore and reset storms are present.

2) There were 7 cluster locations of rip channel activity, which occurred even after multiple reset storms changed the beach state. These clusters were shown to be significant at the 95 percent confidence level. The evidence of rip channels developing in similar locations even after the destruction or reconfiguration of the sand bar means there was something driving the formation of rip channels in these locations. This could be explained by the ridge and swale topography creating a wave forcing that caused bar migration at Casino Beach. Due to the wave forcing, as the bar migrated and attached to the shoreline at certain locations creating a transverse bar and rip state the rip channels developed. The bar appeared to have attached at similar locations throughout the year meaning the rip locations should be in similar locations as well.
3) All of the rip channels developed in a northwest to southeast direction and the rips developed on average when the wave height was 0.90 m, a wave angle from the southeast to the northwest, and a southerly wind.
4) The wave and wind climate conducive for rip current development occurred throughout most of the year. However, large frontal storms did not allow for consistent, steady bar migration and rip channel development until April and May. Meaning the majority of rips did not occur until spring.

Further research needs to be conducted to further understand how and why the rip currents at Casino Beach occur in the 7 distinct clusters. Further research is also needed to determine if those 7 clusters of rip current development occurred only for the year examined or if they are consistent over multiple years and following multiple major storms (hurricanes). Also, further research is needed to determine if the high frequency of rip currents at Casino Beach in April and May are a common occurrence or just a product of the reset storms that occurred throughout the year. It could have been a product of the specific year examined.

REFERENCES

Aagaard, T., B. Greenwood & J. Nielsen (1997) Mean currents and sediment transport in a rip channel. *Marine Geology,* 140, 25-45.

Aarninkhof, S. G. J., I. L. Turner, T. D. T. Dronkers, M. Caljouw & L. Nipius (2003) A video-based technique for mapping intertidal beach bathymetry. *Coastal Engineering,* 49, 275-289.

Bagnold, R.A. (1946) Motion of waves in shallow water. Interaction between waves and sand bottoms. Proceedings of the Royal Society of London A 187:1-18.

Barrett, G. (2011) Variation in Bar Morphology: Implications for Rip Current Development at Pensacola Beach. Master's Thesis. Texas A&M University.

Barrett, G. & C. Houser (2012) Identifying Hotspots of Rip Current Activity Using Wavelet Analysis at Pensacola Beach, Florida. *Physical Geography,* 33, 32-49.

Bowen, A. J., D. L. Inman & V. P. Simmons (1968) Wave 'Set-Down' and Set-Up. *J. Geophys. Res.,* 73, 2569-2577.

Bowman, D., D. S. Rosen, E. Kit, D. Arad & A. Slavicz (1988) Flow characteristics at the rip current neck under low energy conditions. *Marine Geology,* 79, 41-54.

Brander, R. W. (1999) Field observations on the morphodynamic evolution of a low-energy rip current system. *Marine Geology,* 157, 199-217.

Brander, R. W. & A. D. Short (2000) Morphodynamics of a large-scale rip current system at Muriwai Beach, New Zealand. *Marine Geology,* 165, 27-39.

--- (2001) Flow Kinematics of Low-Energy Rip Current Systems. *Journal of Coastal Research,* 17, 468-481.

Claudino-Sales, V., P. Wang & M. H. Horwitz (2008) Factors controlling the survival of coastal dunes during multiple hurricane impacts in 2004 and 2005: Santa Rosa barrier island, Florida. *Geomorphology,* 95, 295-315.

Dean, R. G. & T. L. Walton. 2009. Wave Setup. In *Handbook of Coastal and Ocean Engineering,* ed. Y. C. Kim. Singapore: World Scientific Publishing Co. Pte. Ltd.

Gensini, V. & W. Ashley (2009) An examination of rip current fatalities in the United States. *Natural Hazards*.

Guza, R.T., and A. J. Bowen (1976) Resonant interactions of waves breaking on a beach. Proc. 15 Conference Coastal Engineering. 560-579.

Guza, R. T., and A. J. Bowen (1981) On The Amplitude of Beach Cusps, *J. Geophys. Res.*, 86(C5), 4125–4132,

Guza, R. T. & E. B. Thornton (1981) Wave Set-Up on a Natural Beach. *J. Geophys. Res.,* 86, 4133-4137.

Haller, M. C., R. A. Dalrymple & I. A. Svendsen (2002) Experimental study of nearshore dynamics on a barred beach with rip channels. *Journal of Geophysical Research C: Oceans,* 107, 14-1-14-21.

Holland, K. T., R. A. Holman, T. C. Lippmann, J. Stanley & N. Plant (1997) Practical use of video imagery in nearshore oceanographic field studies. *Oceanic Engineering, IEEE Journal of,* 22, 81-92.

Holman, R.A. (1981) Infragravity energy in the surf zone. Journal of Geophysical Research. 86.

Holman, R. A., G. Symonds, E. B. Thornton & R. Ranasinghe (2006) Rip spacing and persistence on an embayed beach. *Journal of Geophysical Research C: Oceans,* 111.

Houser, C., G. Barrett & D. Labude (2011) Alongshore variation in the rip current hazard at Pensacola Beach, Florida. *Natural Hazards,* 57, 501-523.

Houser, C., N. Caldwell & K. Meyer-Arendt. 2011. Rip Current Hazards at Pensacola Beach, Florida. In *Rip Currents: Beach Safety, Physical Oceanography, and Wave Modeling,* eds. S. Leatherman & J. Fletemeyer. Boca Raton: CRC Press.

Houser, C. & S. Hamilton (2009) Sensitivity of post-hurricance beach and dune recovery to event frequency. *Earth Surface Processes and Landforms,* 34, 613-628.

Houser, C., C. Hapke & S. Hamilton (2008) Controls on coastal dune morphology, shoreline erosion and barrier island response to extreme storms. *Geomorphology,* 100, 223-240.

Huntley, D. A. & A. D. Short (1992) On the spacing between observed rip currents. *Coastal Engineering,* 17, 211-225.

Hyne, N. J. & H. G. Goodell (1967) Origin of the sediments and submarine geomorphology of the inner continental shelf off Choctawhatchee bay, Florida. *Marine Geology,* 5, 299-313.

Kroon, A., M. A. Davidson, S. G. J. Aarninkhof, R. Archetti, C. Armaroli, M. Gonzalez, S. Medri, A. Osorio, T. Aagaard, R. A. Holman & R. Spanhoff (2006) Application of remote sensing video systems to coastline management problems. *Coastal Engineering,* 54, 493-505.

Lascody, L. (1998) East central Florida rip current program. *Nat Weather Dig* 22.

Longuet-Higgins, M. S. (1983) Wave Set-Up, Percolation and Undertow in the Surf Zone. *Proceedings of the Royal Society of London. A. Mathematical and Physical Sciences,* 390, 283-291.

Longuet-Higgins, M. S. & R. W. Stewart (1963) A note on wave set-up. *Journal of Marine Research,* 21, 4-10.

Lushine, J. B. 1991. Rip currents. Human impact and forecastibility. In *Coastal Zone: Proceedings of the Symposium on Coastal and Ocean Management*, 3558-3569.

MacMahan, J., J. Brown & E. Thornton. 2009. Low-Cost Handheld Global Positioning System for Measuring Surf-Zone Currents. In *Journal of Coastal Research*, 744-754. Allen Press Publishing Services Inc.

MacMahan, J., A. J. H. M. Reniers, E. B. Thornton & T. P. Stanton (2004) Infragravity Rip Current Pulsations. *Journal of Geophysical Research,* 109.

MacMahan, J. H., E. B. Thornton & A. J. H. M. Reniers (2006) Rip current review. *Coastal Engineering,* 53, 191-208.

MacMahan, J. H., E. B. Thornton, T. P. Stanton & A. J. H. M. Reniers (2005) RIPEX: Observations of a rip current system. *Marine Geology,* 218, 113-134.

NOAA National Climatic Data Center, State of the Climate: Tornadoes for Annual 2010, published online December 2010, retrieved on January 10, 2012 from http://www.ncdc.noaa.gov/sotc/tornadoes/2010/13.

NOAA. NOAA's Rip Current Program: forecasting and raising public awareness about the drowning machine, published online August 2002, retrieved on January 11, 2012 from http://www.magazine.noaa.gov/stories/mag48.htm

Sallenger Jr, A. H., R. A. Holman & W. A. Birkemeier (1985) Storm-induced response of a nearshore-bar system. *Marine Geology,* 64, 237-257.

Shibayama, T. 2009. Coastal processes: concepts in coastal engineering and their applications to multifarious environments In *Advanced Seriers on Ocean Engineering*. Singapore: World Scientific Publishing Co. Pte. Ltd.

Short, A. D. (1985) Rip-current type, spacing and persistence, Narrabeen Beach, Australia. *Marine Geology,* 65, 47-71.

Short, A. D. & C. L. Hogan (1994) Rip currents and beach hazards: their impact on public safety and implications for coastal management. *Journal of Coastal Research,* 12, 197-209.

Smit, M. W. J., S. G. J. Aarninkhof, K. M. Wijnberg, M. González, K. S. Kingston, H. N. Southgate, B. G. Ruessink, R. A. Holman, E. Siegle, M. Davidson & R. Medina (2007) The role of video imagery in predicting daily to monthly coastal evolution. *Coastal Engineering,* 54, 539-553.

Sonu, C. J. (1972) Field Observation of Nearshore Circulation and Meandering Currents. *J. Geophys. Res.,* 77, 3232-3247.

Stone, G. W. & F. W. Stapr. Jr (1996) A Nearshore Sediment Transport Model for the Northeast Gulf of Mexico Coast, U.S.A. *Journal of Coastal Research,* 12, 786-793.

Stone, G. W., F. W. Stapor, J. P. May & J. P. Morgan (1992) Multiple sediment sources and a cellular, non-integrated, longshore drift system: Northwest Florida and southeast Alabama coast, USA. *Marine Geology,* 105, 141-154.

Svendsen, I. A. (1984) Wave heights and set-up in a surf zone. *Coastal Engineering,* 8, 303-329.

Thornton, E. B., J. MacMahan & J. A. H. Sallenger (2007) Rip currents, mega-cusps, and eroding dunes. *Marine Geology,* 240, 151-167.

van Enckevort, I. M. J. & B. G. Ruessink (2003) Video observations of nearshore bar behaviour. Part 2: alongshore non-uniform variability. *Continental Shelf Research,* 23, 513-532.

Wiberg, P. L. 2005. Wave-Current Interaction. In *Encyclopedia of Coastal Science,* ed. M. L. Schwartz, 883. Dordrecht, The Netherlands: Springer.

Wright, L. D. & A. D. Short (1984) Morphodynamic variability of surf zones and beaches: A synthesis. *Marine Geology,* 56, 93-118.